ESCUELA DE INGENIERÍA DE FUENLABRADA

Biomedical Engineering

BACHELOR THESIS

T-WAVE ALTERNANS DETECTION: A MACHINE LEARNING AND DEEP LEARNING APPROACH IN PYTHON

Author: Álvaro Santiago Sosa García

Supervisor: Rebeca Goya Esteban

Acedemic year 2023/2024

Dedicated to my Uncle Miguel.

Acknowledgments

This work represents the end of an adventure that began 4 years ago, full of excitement, and culminated in this way, making me a biomedical engineer. During these 4 years, there have been many experiences lived and difficulties faced, and in these lines I want to thank all the people who have made it possible.

Firstly, I want to thank my family, Mom, Dad, and my brother Miguel, who have been the support I leaned on when things didn't go well. Thank you for everything you teach me every day, you are my role models.

Secondly, I want to thank my classmates and especially the "Cabrix". You have been that group of friends to turn to when things are going well, but especially when situations become difficult. I also want to thank Carla for the love and support that she has gave me through this last year.

Thirdly, thanks to all the teachers who have accompanied and taught me during this period.

Fourthly, I want to thank my supervisor, Rebeca, for everything taught and for making the development of this work something simpler and more enjoyable.

Finally, I want to dedicate this work entirely to my uncle Miguel. I hope you can see from wherever you are the professional I have become and will become. We all miss you so much.

Abstract

Sudden Cardiac Death (SCD) is a significant global health issue, accounting for a substantial proportion of cardiovascular disease-related mortality. SCD often results from ventricular arrhythmias, which can occur without prior warning, making early detection crucial. One of the promising indicators for predicting SCD is **T-wave alternans (TWA)**, which are subtle variations (order of μV) in the amplitude or shape of the T-wave in an electrocardiogram (ECG). Detecting TWA is essential as it can help identify individuals at high risk of SCD, enabling timely interventions.

In this study, the creation of a comprehensive database by collecting and preprocessing ECG signals was developed. The **preprocessing steps** included the addition of alternans, removal of baseline wander, delineation of the ST-T complex, heartbeat windowing, ST-T alignment, background subtraction, linear filtering, and building the signals dataframe. These steps ensured the quality and consistency of the data used for analysis.

Relevant **features were extracted** from the preprocessed ECG signals, highlighting the K_{score}, V_{alt} and the noble cumsum-based feature, to improve the detection accuracy of TWA. Various **machine learning algorithms** were employed, including Logistic Regression (LR), Decision Tree (DT), Random Forest (RF), and Support Vector Machine (SVM), to evaluate their performance in detecting TWA.

Furthermore, we implemented **advanced deep learning techniques**, specifically Long Short-Term Memory (LSTM) networks and a hybrid CNN-LSTM architecture. Our results demonstrated that **LSTM networks** outperformed other models, achieving an outstanding **accuracy of 94.08%,** which is the highest performance reported in the literature for TWA detection.

This research highlights the potential of LSTM networks in improving the early detection of TWA, thereby contributing to the prevention of SCD. The findings suggest that incorporating deep learning models, particularly LSTM networks, can significantly enhance the accuracy and reliability of TWA detection, offering a robust tool for clinicians in the fight against SCD.

Contents

List of Figures

List of tables

Chapter 1

Introduction

1.1 Motivation

Cardiovascular diseases represent one of the main reasons for morbidity and mortality throughout the world. In fact, cardiovascular disease remains the most common cause of death worldwide. In this sense, the 2013 Global Burden of Disease study estimated that cardiovascular disease is responsible for **17.3 million deaths globally every year** [1].

Between some of the main manifestations of these diseases, **sudden cardiac death (SCD)** emerges as a particularly alarming one. SCD is an unexpected sudden death due to a heart condition. SCD affects heavily on the health care system, being the leading cause of death in western countries (15-20%) [2], and responsible for the majority of deaths associated to cardiovascular diseases. Against this reality, it is crucial to approach this problem with the design and implementation of algorithms and tools that allow the screening and prevention of this phenomena, and consequently, its big impact in our health care system.

The development of techniques in the screening of population have been studied and applied in order to diminish the risk of SCD. Clinical evaluation of the electrocardiogram (ECG), cardiac magnetic resonance (CMR) or endomyocardial biopsy are some of the main mechanisms of screening used nowadays [3].

However, the existing techniques do not allow enough reliable results as SCD is still a mayor cause of death worldwide. In this sense, **T-wave alternats (TWA)** appears as a new promising technique. TWA is a fluctuation of the ST–T complex of the surface ECG on an every–other–beat basis. This technique has shown to improve the results regarding specificity and sensitivity in the detection of various

cardiovascular diseases like Ventricular Fibrillation (VF) and especially, SCD [4].

Nevertheless, the work on analyzing them becomes really hard; the imperceptible shape of the TWA to the human eye due to the small amplitude of the wave, the noise, and the overlapping with other waves makes the detection of them by physicians almost impossible. A carefully designed framework for the TWA detection is required.

With this study, it is intended to develop a solid pipeline for the detection of TWA with the goal of improving the already obtained results and redefine a new gold-standard in the prevention of SCD.

It is important to remark that this project grows as a continuation of the work developed in "Machine Learning approach for TWA detection relying on ensemble data design" by Fernández-Calvillo et al. [4]. With this project it is aimed to use these basis in the development of new techniques to identify TWA and stratify cardiac risk.

The entire code developed in this work can be further analysed through the following link: TFG-CODE-LINK.

1.2 Goals

The main goal of this project is to design a pipeline for the detection of SCD based on the idea that TWA are a powerful and reliable indicator of this pathology. In order to develop this idea, there was a clear necessity of stating accurate and pragmatic sub-goals that would build together a final result. It was defined, therefore, six main sub-goals in this project.

1. **Understanding on the physiological and pathological basis behind T-wave alternans.**

   This involves delving into the mechanisms underlying T-wave alternans, which can be indicative of cardiac arrhythmias or other heart conditions. TWA is a very special phenomena which need to be explored through the available bibliography to build the project over a solid clinical mind.

2. **Building of an adequate database for TWA detection.**

   Once the knowledge around the pathopysiological basis surrounding TWA is consolidated, it is necessary to build and design a machine-learning appropriated database.

This involves collecting ECG from different patients and from different reliable databases in order to build a self-created database specialized in alternans detection.

3. **Development of ECG preprocessing techniques.**

   Once our database is correctly designed and understood and before diving into the alternans analysis, raw ECG signals need from preprocessing stages in order to be able to extract the maximum information from it. Techniques such as baseline wander elimination, windowing or linear filtering will be used during this stage.

4. **Extraction of features on the preprocessed signals.**

   Once preprocessing is complete, features relevant to TWA regarding on their shape and behaviour are extracted from the ECG signals. These features provide the basis for subsequent machine learning analysis.

5. **Development of Machine Learning (ML) techniques for the detection of TWA.**

   Various ML algorithms, such as support vector machines, random forests, and logistic regression are trained on the extracted features to classify ECG segments as either exhibiting TWA or not. Performance metrics are then compared to identify the most effective approach.

6. **Development of Recurrent Neural Networks (RNN) for the detection of TWA.**

   RNNs, particularly suited for sequential data like ECG signals, are explored to assess their effectiveness in detecting TWA. The complete preprocessed ECG data is fed into the RNN model to capture temporal dependencies and potentially improve detection accuracy.

1.3 Methodology and memory structure

In order to achieve the previously mentioned goals, the following methodology was used:

1. **Bibliographic review**: Before entering on the technical aspects of the project a deep understanding of the medical context together with a comprehension of the TWA phenomena was required

2. **Creation of a signal database**: The lack of properly annotated databases in the TWA field made necessary the creation of an own database for posterior analysis.

3. **Preprocessing of the database and creation of a ML/DL-oriented database**: After the creation the signals would precise a specialized preprocessing to highlight the alternans presence. Then, a data frame for the experimental part should be constructed.

4. **Comparison of the different models**: Different ML models and DL architectures are conducted to get a consistent visualization on the best models for this particular problem.

5. **Conclusion**: After analyzing the results obtained with the models, a proper conclusion should be stated on the best approaches for this problem together with future work on the field to be done.

The structure of the document is the following:

- **Chapter 1: Introduction.**
- **Chapter 2: Background.**
- **Chapter 3: Data analysis.**
- **Chapter 4: Experiments.**
- **Chapter 5: Results and Discussion.**
- **Chapter 6: Conclusions, future work and competencies acquired.**
- **Chapter 7: Appendices.**

Chapter 2

Background

2.1 Sudden cardiac death

Sudden cardiac death (SCD) is a pathology characterized by the unexpected death from a cardiac cause within a short time period, commonly less than 1 hour from the onset of symptoms when witnessed, or in the case it is not witnessed, an unexpected death from a cardiovascular cause where the individual was observed to be alive within the previous 24 hours. In any case, the person was not apparently suffering from any prior condition [5].

The epidemiology of SCD has been an intense field of study due to its significant impact in public health and its capability to affect individuals from any age or health condition. SCD remains as the **main cause of death in western countries** with an incidence of between 15-20%. In North America and European populations, the annual incidence rate of this conditions appears to be around 50-100 per 100.000 inhabitants in studies developed from 2005 to 2015 [6].

The majority of sudden cardiac death cases are due to undetected cardiovascular diseases, including congenital heart defects in younger individuals and **coronary artery disease** in those over 35 years old. Coronary artery disease accounts for 70-80% of SCD cases, with **ventricular arrhythmias** such as ventricular tachycardia (VT) and ventricular fibrillation (VF) being the primary cause. Additionally, other types of syndromes and pathologies such as inherited arrhythmias or cardiomyopathies can also lead to SCD as it can be seen in figure 2.1 [7].

SCD can be challenging to classify accurately due to factors such as unwitnessed events, accounting for 40% of cases [8]. The advent of monitoring capabilities, particularly with implantable cardioverter-defibrillators (ICDs), has shed light on the

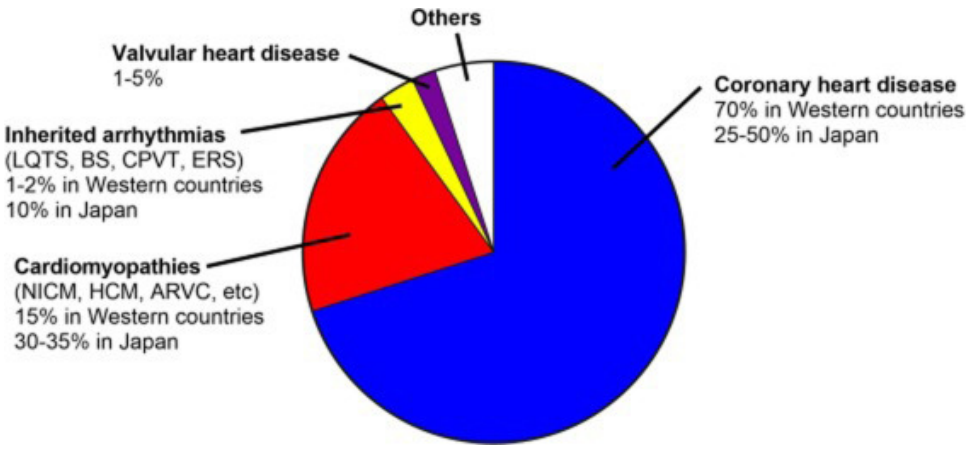

Figure 2.1: Main causes of SCD in Western countries and Japan [7].

limitations of classifying sudden deaths based solely on clinical circumstances. Only an ECG or a ventricular electrogram recorded from an implanted device at the time of death can definitively reveal information about an arrhythmia. Prodromal symptoms, which can be nonspecific, including chest pain suggesting ischemia, palpitations indicating tachyarrhythmia, or dyspnea suggesting congestive heart failure, are often present but are only suggestive rather than conclusive. For these reasons, total mortality, rather than classifications of cardiac and arrhythmic mortality, should be used as primary objectives for many outcome studies [5].

All of this has made SCD a phenomenon of study in the scientific community, leading to the development of methods for the prevention and screening of it. These testing techniques can be mainly divided in invasive or non-invasive. Invasive methods include electrophysiological studies (EPS), while noninvasive methods encompass conventional ECG, medical imaging techniques, long-term ECG monitoring (Holter), and other tests such as genotype determination or stress tests for specific cardiopathies.

EPS involves the use of intracardiac catheters to assess internal cardioelectric activity and induce ventricular arrhythmias. However, its usefulness is limited to certain conditions like ischemic cardiopathy and Brugada syndrome, with weak validation in other cardiopathies. Conventional ECG provides graphical representation of cardiac electrical activity and can aid in diagnosing underlying cardiopathies and identifying elements suggestive of increased SCD risk, such as QT interval prolongation or bundle-branch blocks. Medical imaging techniques like echocardiography help estimate left ventricular ejection fraction (LVEF), which is a significant risk factor for SCD in various cardiopathies. Additionally, cardiac nuclear magnetic resonance can assess myocardial fibrosis, associated with ventricular arrhythmias. Long-term ECG monitoring (Holter) detects arrhythmic events like ventricular premature beats and non-sustained ventricular tachycardia, providing valuable information for SCD risk assessment. Other tests, such as ECG signal averaging and baroreflex sensitivity, offer insights into arrhythmic substrate and autonomic function regulation, respectively, but their clinical utility for SCD risk prediction is

limited or under investigation [9].

Moreover, the analysis of various algorithms and computational indexes have been identified to be useful in the prediction and stratification of SCD. Among them, we find the HRT indexes, which describe small fluctuations in the ECG, HRV , which measures temporal variation between sets of consecutive cardiac beats, reflecting autonomic nervous system control or the TWA [9].

All this techniques have tried to approach a reliable predictor and detector for SCD prevention. However, the clinical studies have shown a low efficiency in terms of specificity and positive predictive value of this techniques [10].

The **lack of a gold standard** for the detection and stratification of cardiac risk builds up a big necessity in the field. New studies and investigations in the field will be needed in future years.

2.2 Heart, electrocardiogram and arrhythmia

2.2.1 Heart

The heart functions as a rhythmic electromechanical pump, relying on the generation and spread of action potentials, followed by relaxation and a refractory period before the next impulse. Action potentials in the heart reflect the activation and deactivation of various ion channels carrying inward (Na+ and Ca2+) and outward (K+) currents. These channels differ in expression across heart regions, resulting in distinct action potential waveforms, crucial for orderly propagation of activity and normal cardiac rhythm generation. Changes in channel function, whether inherited or acquired, can disrupt action potential repolarization, potentially leading to life-threatening arrhythmias. Thus, there's significant interest in comprehending the mechanisms governing cardiac repolarization and rhythm formation [11].

As it can be overviewed in figure 2.2, cardiac electrical activity begins with pacemaker cells in the sinoatrial (SA) node and then travels through the atria to the atrioventricular (AV) node. After a short delay at the AV node, the excitation spreads through the conducting Purkinje fibers to the apex of the heart and into the ventricular myocardium. In each specialized region, excitation triggers action potential generation, which is followed by relaxation and a refractory period before the next impulse is generated and propagated. Cardiac action potentials are fundamental to understanding the generation and propagation of the heart rhythm, and they are reflected in the ECG.

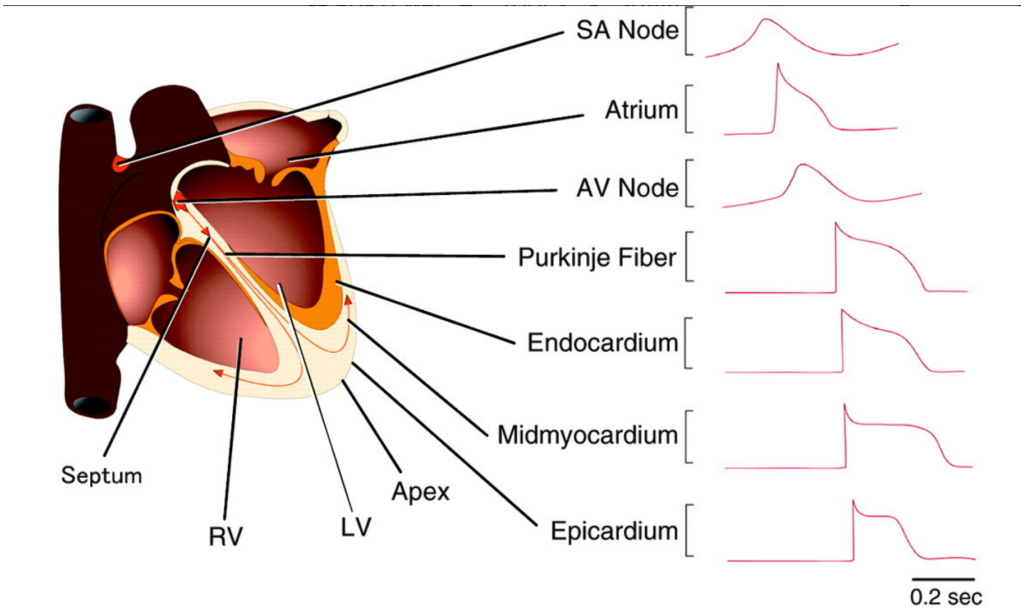

Figure 2.2: Schematic of a human heart with illustration of typical action potential waveforms recorded in different regions [11].

2.2.2 Electrocardiogram

ECG is one of the most common noninvasive diagnostic tools that can provide useful information regarding a patient's health status. In figure 2.3,the main parts of it are represented , which are the result of the cardiac electrical activity.

- **P wave**: Represents the depolarization of the atria initiated by the firing of the SA node.
- **PR interval**: The segment from the beginning of the P wave to the beginning of the QRS complex. It indicates the time it takes for the electrical impulse to travel from the sinoatrial node to the atrioventricular node.
- **QRS complex**: Reflects the depolarization of the ventricles.The Q wave represents initial septal depolarization, the R wave signifies depolarization of the main mass of the ventricles, and the S wave represents the completion of ventricular depolarization
- **ST segment:** The period between the end of the QRS complex and the beginning of the T wave. It represents the early repolarization phase of the ventricles.
- **T wave**: Indicates the repolarization of the ventricles.
- **TP segment**: The interval between the end of the T wave and the beginning of the next P wave. It represents the period when the ventricles are in electrical rest before the next contraction.

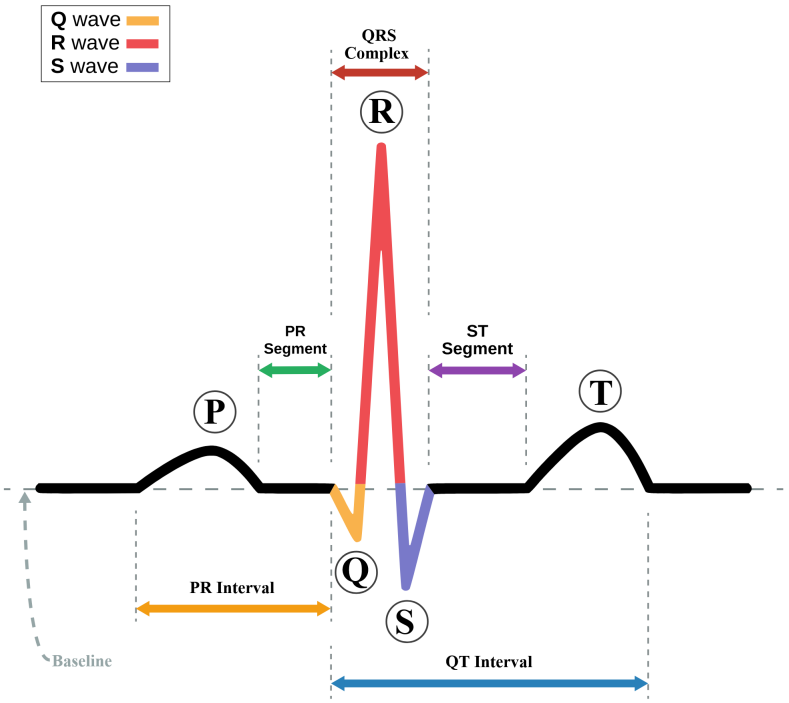

Figure 2.3: Normal sinus rhythm electrocardiogram representation.

It is important to note that changes in action potentials, whether due to genetic or acquired disorders, can alter the normal ECG pattern and predispose to dangerous cardiac arrhythmias. Therefore, the ECG not only provides a visual representation of the heart's electrical cycle but also serves as a crucial tool for detecting abnormalities in cardiac electrical activity:

The study of ECG's has seen significant advancements with the integration of deep learning and machine learning techniques [12], revolutionizing the way we interpret cardiac data and predict potential cardiac events such as sudden cardiac death. In this project, the study of T-wave alternats will be extremely correlated to the **understanding and application of DL and ML techniques** around the ST segment.

2.2.3 Cardiac Arrhythmia

Cardiac arrhythmias refer to deviations or irregularities in the typical activation or beating pattern of the heart's myocardium. Normally, the sinus node initiates a depolarization wave that spreads through the atria, then through the atrioventricular (AV) node, and finally propagates over the His-Purkinje system to depolarize the ventricles in a coordinated manner. Various types of cardiac arrhythmias can occur, disrupting this normal rhythm. The standard rhythm of the heart is termed normal

sinus rhythm (NSR), which can be disrupted by failures in automaticity, such as in sick sinus syndrome (SSS), or by inappropriate sinus tachycardia. Premature atrial contractions and premature ventricular contractions can also occur during the heart's beating process [13].

The severity of cardiac arrhythmias depends on whether structural heart disease is present. Conditions such as atrial fibrillation (AF) are considered benign arrhythmias. However, in patients with coronary heart disease or severe left ventricular dysfunction, arrhythmias can contribute to heart failure or sudden cardiac death.

Arrhythmias encompass a wide array of irregular heart rhythms, each presenting unique challenges and implications for cardiac health. While there are numerous types of arrhythmias, for the purpose of this discussion, we will focus primarily on ventricular arrhythmias due to their direct association with SCD.

- **Ventricular Tachycardia (VT)**: Ventricular tachycardia is a disorder of the heart rhythm caused by abnormal electrical signals in the ventricles. A normal healthy heart typically beats between 60 and 100 times per minute at rest. When experiencing ventricular tachycardia, the heart beats faster than normal, usually at a rate of 100 or more beats per minute. In figure 2.4, a typical representation in an ECG of this pathology is represented.
- **Ventricular fibrillation (VF)**: Ventricular fibrillation is a serious heart condition in which the ventricles of the heart experience rapid and uncoordinated contractions instead of rhythmic and coordinated contraction. This significantly interferes with the heart's ability to pump blood effectively to the entire body, which can lead to a rapid and potentially fatal decrease in blood pressure and blood circulation. During ventricular fibrillation, the heart muscle does not contract synchronously, resulting in chaotic electrical activity in the ventricles instead of a stable heart rhythm. As a result, the heart cannot pump blood effectively, and the supply of oxygen to vital organs is rapidly compromised.

Cardiac arrhythmia's are therefore a key factor in the development of cardiac diseases and sudden cardiac death. Its detection is vital for a better prognosis. Several techniques are used nowadays to diagnose them. Deep Learning in the ECG in Somani et al. [14], smart and wearable devices in Sajeev et al. [15], or even mobile applications.

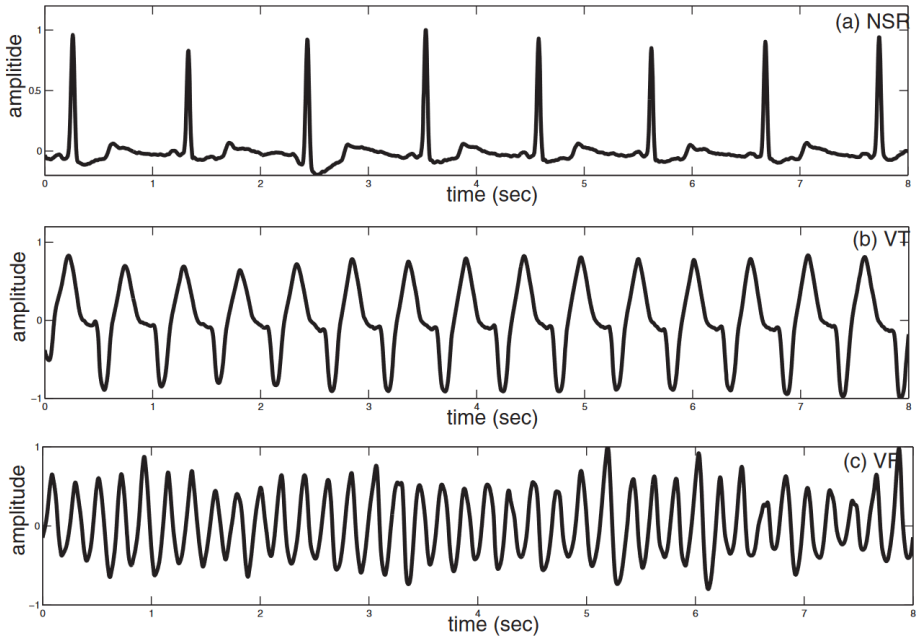

Figure 2.4: Characteristics of different variety of ECG signals (a) NSR episode, (b) VT episode, and (c) VF episode [16].

2.3 T-wave alternans

2.3.1 Introduction to cardiac alternans

Cardiac alternans refers to a condition characterized by a **periodic beat-to-beat oscillation** in electrical activity and the strength of cardiac muscle contraction at a constant heart rate. The clinical manifestations of alternans occur in many settings in which arrhythmias are also common; however, its origin can be followed to the cellular and subcellular level [17].

Cardiac alternans can be broadly classified into two types: electrical and mechanical. Electrical alternans occurs due to a fundamental alteration in the electrical conduction within the heart muscle manifested as a consistent change in the shape of the ECG waveform occurring every other heartbeat, while mechanical alternans results from a fluctuation in the mechanical function of the heart.

In 1872, Traube [18] made the initial observation of a fascinating phenomenon: beat-to-beat oscillations in arterial pressure occurring while the heart rate remained steady. This phenomenon, initially termed “pulsus alternans”, eventually became recognized as mechanical alternans. With the advent of the ECG, similar beat-to-beat alternations in the heart’s electrical activity were documented in laboratory in animals and humans, known as repolarization or **T-wave alternans**.

This TWA were firstly described in 1908 by Hearing [19]. After that, Thomas Lewis [20] recognized that cardiac alternans could occur in normal hearts as a result of **marked acceleration of heart rate** and also in the impaired or intoxicated myocardium. Despite that, Kalter and Schwartz [21] reviewed clinical ECG of around 6000 patients and found five cases of human eye visible TWA, the low incidence and the difficulty in the analysis left TWA as a forgotten topic for many years.

Over time, it became evident that cardiac alternans, whether mechanical or electrical, signaled an increased risk of atrial and ventricular arrhythmias and sudden cardiac death across various pathophysiological conditions such as diabetes, ischemia, myocardial infarction, and chronic heart failure [17].

Today, TWA are defined as a **beat-to-beat fluctuation** in the amplitude, waveform, or duration of the **ST-segment or T-wave** [22]. TWA testing serve as valuable prognostic tools for assessing arrhythmia and sudden cardiac death risk in chronic heart failure patients, aiding in the selection of appropriate antiarrhythmic therapies.

A common picture of this phenomena can be seen in figure 2.5

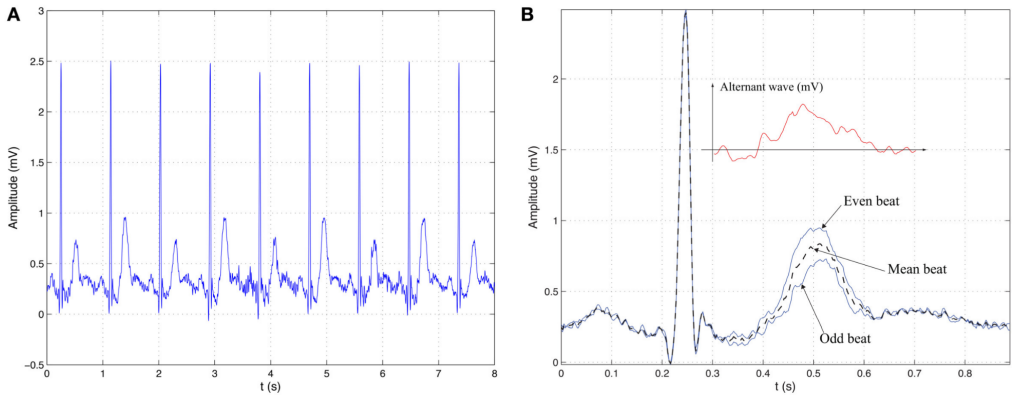

Figure 2.5: Illustrative example of TWA. (A) ECG signal with periodic pattern alternation in the repolarization segment with a period of two beats. (B) Visual interpretation of TWA as the difference between the averaged event beat and the averaged odd beat [9].

2.3.2 Pathopyhsiology on T-wave alternans

The detection of TWA on the surface ECG may not be easily distinguishable due to their microvolt nature range. This, underscores the importance of considering the cellular-level effects of TWA despite its minimal visual impact on surface recordings. This can be properly appreciated in figure 2.6.

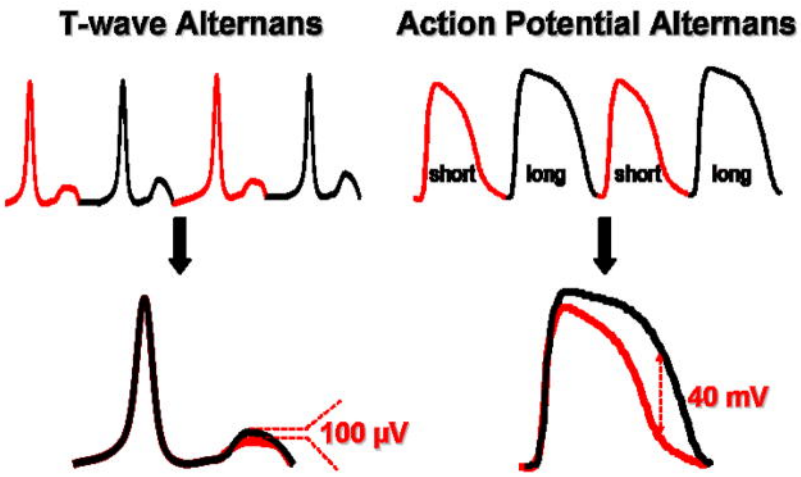

Figure 2.6: Cellular basis for T-wave alternans. **Upper Panel**: The onset of T-wave alternans on the ECG arises from beat-to-beat alternation of the action potential at the level of the single cardiac myocyte. **Lower Panel**: The magnitude of action potential alternans (millivolt) is several orders of magnitude larger than T-wave alternans (i.e. microvolt) on the ECG [23].

Several studies have concluded about the need of a controlled increase of the heart rate (HR) as TWA is a rate-dependent property of the heart. In this sense, above a specific HR threshold, TWA increases monotonically. Thus, **why is TWA dependent on HR?**

Understanding HR dependence of TWA involves delving into the cellular and molecular mechanisms governing the development of repolarization alternans within individual cardiac myocytes. Two primary hypotheses have been posited to elucidate this phenomenon, both of which offer insights into why TWA is influenced by HR. APD restitution hypothesis and calcium cycling hypothesis [24].

- **APD restitution hypothesis**: The reduction in action potential duration (APD) that occurs with increasing HR, known as action potential restitution, is believed to be a mechanism aimed at preserving diastolic filling time at faster HRs. This process entails a direct relationship between the APD of one heartbeat and the diastolic interval (DI) preceding it. Action potential restitution can elucidate the self-perpetuating nature of APD alternans: a short DI leads to APD shortening, which then extends the DI preceding the subsequent beat, resulting in APD lengthening and subsequent DI shortening in a repetitive cycle [25, 26].

  Theoretical models propose that repolarization alternans arises when the slope of the dynamic APD restitution curve (APD vs. DI) exceeds unity as can be seen in figure 2.7. Simulation studies suggest that the precise HR required to induce TWA can be directly predicted from the restitution relationship. While the restitution hypothesis provides a valuable theoretical framework for understanding TWA dynamics, experimental evidence supporting it remains somewhat indirect [24].

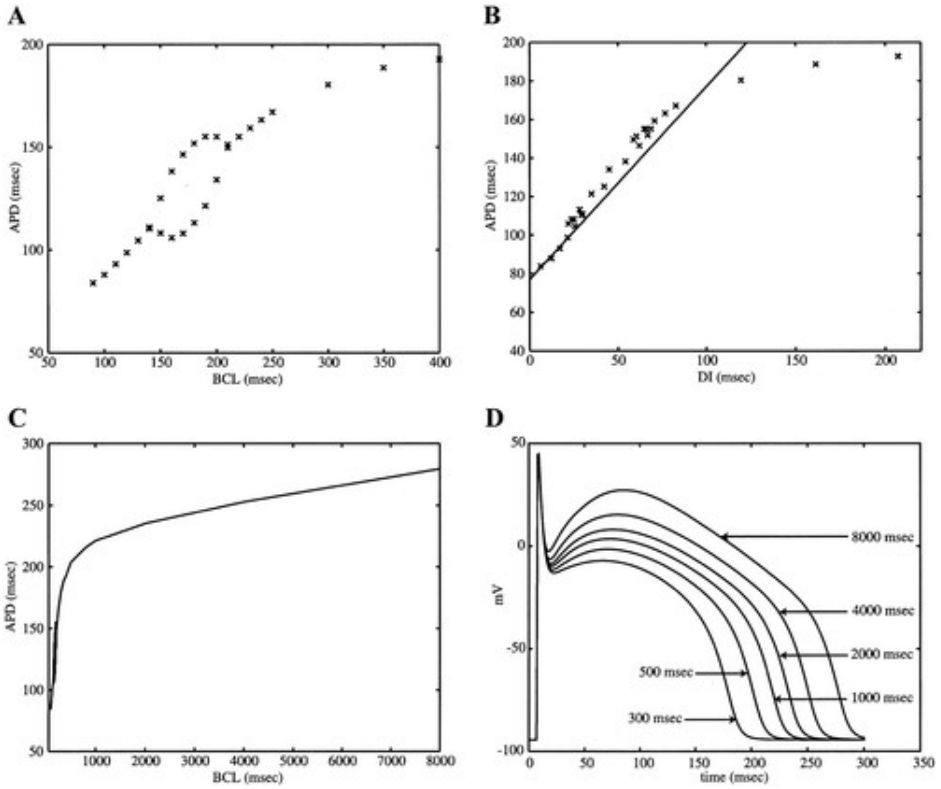

Figure 2.7: Relationship between action potential duration and the pacing cycle length over the range of cycle lengths that produced electrical alternans (400–90 ms;A) and over a wider range of cycle lengths (8,000–90 ms;C). Action potentials generated at several different pacing cycle lengths are shown in D. The model generated electrical alternans over a wide range of pacing cycle lengths, in association with a region of the restitution relation having a slope equal to 1 (B) [27].

- **Calcium cycling hypothesis**: The calcium cycling hypothesis posits that alternans occurs when the HR surpasses the myocyte's ability to cycle calcium effectively on a beat-by-beat basis. Any factor that impedes cellular calcium cycling can trigger alternans even at lower HRs, making alternans a rate-dependent process. In normal conditions, calcium is released from the sarcoplasmic reticulum (SR) through the ryanodine receptor (RyR) complex, leading to myocardial contraction. Relaxation primarily involves the re-uptake of calcium into the SR by sarcoplasmic reticulum Ca^{2+}-ATPase (SERCA2a), with the sodium calcium exchanger (NCX) contributing to diastolic calcium removal from the cytosol.

  According to this hypothesis, during steady-state conditions (e.g., resting HR), the amount of calcium released from the SR must equal SR re-uptake, primarily mediated by SERCA2a. Under such circumstances, calcium alternans will not develop as it can be see in Panel A of figure 2.8. However, sustained disturbances in the myocyte's ability to load SR calcium (e.g., impaired SR calcium reuptake) or release SR calcium can lead to the development of calcium alternans as can be seen in Panels B and C in figure 2.8 [23, 24].

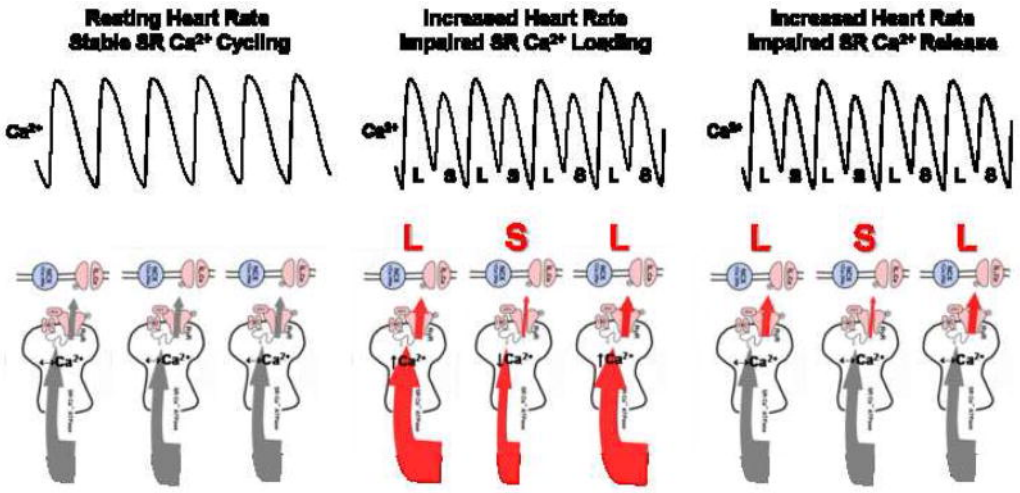

Figure 2.8: Calcium cycling hypothesis. **Panel A**: During steady-state SR Ca^{2+} cycling at resting heart rates Ca^{2+} transient alternans will not develop because SR Ca^{2+} release equals SR Ca^{2+} reuptake. **Panel B**: Impaired SR Ca^{2+} loading, leading to beat-to-beat fluctuation in SR Ca^{2+} content will produce Ca^{2+} transient alternans (i.e. large SR Ca^{2+} release followed by a small SR Ca^{2+} release). **Panel C**: Impaired SR calcium release in the absence of beat-to-beat fluctuation in SR Ca^{2+} content can also produce Ca^{2+} transient alternans [24].

However, it is important to highlight that HR may not be always required for the development of TWA. According to Schwartz et al. [28], Long QT syndrome TWA mediated ventricular arrhythmia are associated with slow HRs. Therefore, HR may not be taken as a unique and only factor that lead to the appearance of TWA.

Apart from this phenomena, there are also other factors that may be related to the appearance of alternans. In [29], it is mentioned that **potassium channels** may have a direct impact in the development of ischemia-induced TWA. The different spatial (epicardial vs. endocardial) sensitivity of K-ATP channel activation during ischemia may be linked to repolarization alternans at the cellular level during regional ischemia. In a porcine model, acute ischemia shortened the APD, therefore, the effects mentioned above on the APD restitution hypothesis are suitable, and therefore the TWA appearance. Furthermore, in [30], connexin-related problems are also seen as factors inducing the TWA creation. **Connexins** are proteins found within cell membranes that control the flow of ions between cells, facilitating cellular communication and conduction. When the body experiences low oxygen levels (hypoxia) or reduced blood flow (ischemia), cellular communication breaks down simultaneously with the onset of ischemic contracture, an increase in calcium levels within the cell [31], rapid depletion of ATP (the cell's energy source) [32], and acidification. This suggests that both reduced excitability and disrupted cellular communication are likely to vary within an ischemic area, potentially causing irregular impulse propagation and leading to alternating areas of excitation.

2.3.3 Relation with cardiac arrythmia and SCD

Numerous studies have shown TWA to be a marker of risk of SCD. In this sense, figure 2.9, perfectly explains it. Spatially **concordant alternans** (which in essence are repolarization alternans occurring with opposite phase between neighboring cells), was shown to be intrinsically related with the arrytmia generation. As we can see in figure 2.9, in a first instant, all myocites alternate in the same phase (this is long (L)-short(S)). This would not appear to be a problem, but it is a required precondition to develop the **discordant alternans**(two spatially discrete sites exhibiting APD alternans at opposite phases [33]). The reality is that as HR surpasses a threshold, as it can be seen in figure 2.10 , a shift in the pattern of the alternans can occur, thus, passing from concordant alternans to discordant alternans.

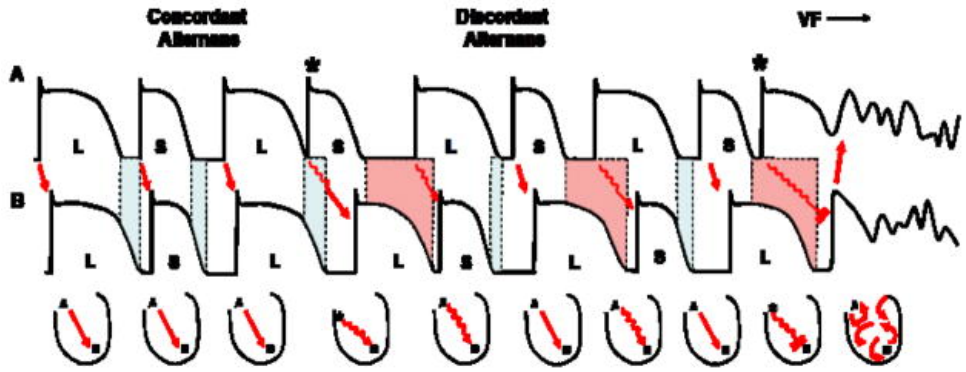

Figure 2.9: Mechanism linking cardiac alternans to arrhythmogenesis [24].

This formation of discordant alternans produces an alteration in the spatial organization of the ventricles, which finally can lead to a VF and ultimately to SCD [24].

Once the relation between alternans and cardiac diseases is clear, a question arises. **Why is there a transformation from concordant alternans to discordant alternans?** Several mechanisms have been identified to cause this shift: 1) conduction velocity restitution 2) inter-cellular uncoupling and 3) spatial heterogeneities of calcium cycling and sarcolemmal repolarization currents [24].

Regarding the **conduction velocity restitution mechanism**, computer modelling studies [34] propose a mechanism for discordant alternans driven by conduction velocity restitution. These simulations, conducted on homogeneous tissue, suggest that conduction velocity restitution alone, or in conjunction with spatial heterogeneities of repolarization, may account for discordant alternans. Specifically, these simulations indicate that while discordant alternans can manifest in the presence of significant heterogeneities of APD restitution within the myocardium, it can also occur in the absence of spatial heterogeneity of APD restitution, provided there is substantial restitution of conduction velocity. In scenarios where conduction velocity restitution is significant, during steady-state pacing, cardiomyocytes distant

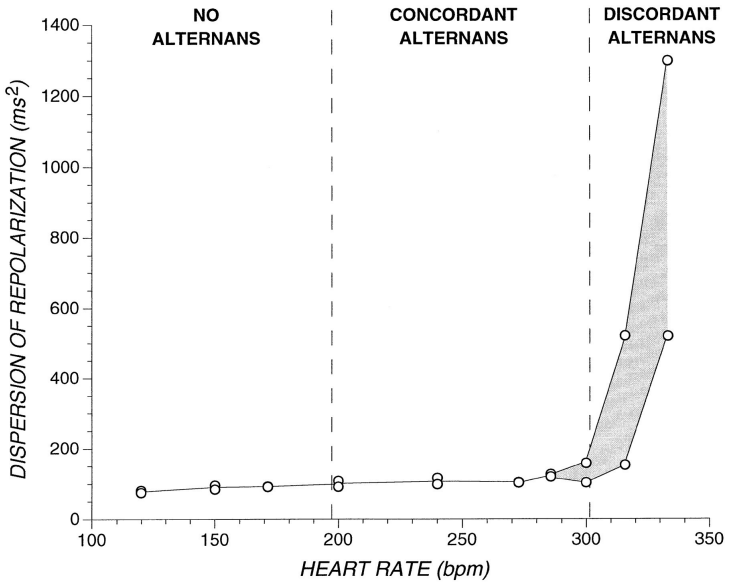

Figure 2.10: Representative experiment demonstrating effect of concordant and discordant alternans on spatial dispersion of repolarization. Note that discordant alternans, but not concordant alternans, causes marked dispersion of repolarization. Experiment done on guinnea-pigs [35].

from the pacing site may experience longer diastolic intervals compared to those in proximity to the pacing site. Consequently, **despite shorter coupling intervals, cells distant from the pacing site might paradoxically exhibit longer action potentials, leading to the emergence of discordant alternans**. Additionally, conduction velocity restitution may occur due to progressive conduction slowing as the coupling interval of a premature stimulus is shortened.

In computer simulations, if a tightly coupled premature stimulus induces pronounced conduction slowing, it introduces spatial heterogeneity of diastolic intervals. This heterogeneity causes each cell to operate on a different point of its APD restitution curve. Consequently, discordant alternans may arise because the premature stimulus alters the phase of some cells but not others, contingent on the point of the APD restitution curve at which the premature impulse arrives [36].

Entering now in the hypothesis associated to the **spatial heteroginities of calcium cycling**, it is now firmly established that spatial heterogeneities exist in cellular calcium handling within the ventricle, contributing to variations in susceptibility to action potential alternans across different regions. Just as intrinsic heterogeneities in cellular calcium cycling and/or repolarization properties can potentially account for spatial differences in susceptibility to action potential alternans, these same heterogeneities could also underlie the development of discordant alternans.

Myocytes that are prone to action potential alternans typically exhibit the slowest time constant for diastolic calcium re uptake and the highest propensity for rate-dependent cytosolic calcium accumulation. This strongly suggests that calcium

cycling plays a pivotal role in determining susceptibility to action potential alternans. Myocytes prone to alternans express significantly lower levels of SERCA2a and RyR compared to alternans-resistant myocytes, indicating a molecular basis for cellular alternans and implicating calcium cycling proteins in this mechanism.

Moreover, it is highly probable that spatial heterogeneities in repolarization and calcium cycling are interconnected. As calcium alternans serves as the source of cellular action potential alternans, spatial variations in calcium cycling may not only explain susceptibility to action potential alternans but also discordant alternans.

This suggests that understanding the intricate interplay between spatial heterogeneities in calcium handling, repolarization, and their influence on action potential dynamics is crucial for elucidating the mechanisms underlying both action potential and discordant alternans [36].

Finally, also **intercellular uncoupling** is seen as a possible mechanism associated. Cardiac myocytes are connected through gap junctions, enabling the exchange of ionic current between them. Generally, this electrotonic coupling serves to standardize repolarization across cells. Conversely, when cells are uncoupled, inherent differences in their electrophysiological properties become more apparent [37]. This uncoupling can significantly affect the spatial variability of repolarization. Moreover, any inclination for neighboring myocytes to alternate with opposite phases due to disparities in calcium cycling properties, APD restitution, etc., is counteracted by electrotonic coupling between these cells. In a guinea pig model of alternans, the introduction of a structural barrier to uncoupled neighboring cells notably facilitated the emergence of discordant alternans as we it can be appreciated in figure 2.11. This suggests that under normal conditions, intercellular coupling electrically diminishes differences in ionic properties that might lead to spatially discordant alternans [36].

These mechanisms are only some of the factors that can lead to the generation of alternans and ultimately, arrythmias or SCD. However, it is important to take into account that these mechanisms are not mutually exclusive and each of them may contribute in a different way to the generation of this phenomena.

2.3.4 TWA detection methods

TWA nature, of the order of μV, make the manual detection of these waves on the surface ECG almost impossible. Therefore, more developed techniques are required to take the challenge of detecting this cardiac phenomena. These techniques include the use of physiological signal processing.

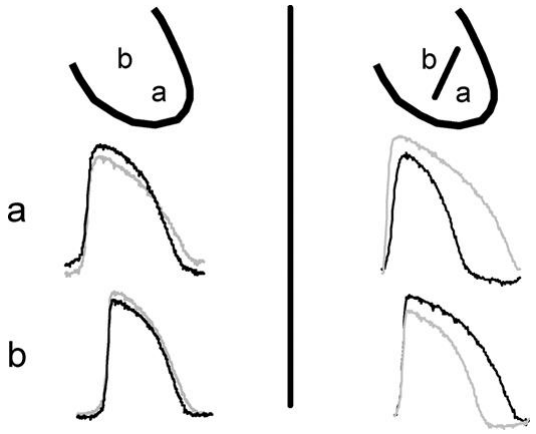

Figure 2.11: Cellular uncoupling from a structural barrier promotes discordant alternans. Left : optical action potentials of epicardial cells from the base (site b) and apex (site a) of a guinea pig heart during two consecutive beats (black and grey) during concordant action potential alternans are shown. Right : the introduction of a structural barrier between the base and apex of the heart promotes discordant alternans, in which action potentials from the base (site b) now alternate out of phase with the apex [38].

As we have seen in 2.10, the HR is a factor highly correlated with the onset of alternans. Therefore, the detection must be done under certain circumstances of HR. In [39], Tanno et al. found that the most suitable HR for alternans detection was around 110 beats per minute (bmp). The onset HR was found to be around 95 bmp and at rates higher than 120 bpm, the specificity regarding the alternans detection was so high. Therefore, elevation of the HR around 110 bmp as a first measure in the alternans detection and, therefore, cardiac risk stratification should be taken into account.

Thus far, numerous techniques have emerged for automatically tracking TWA. Nevertheless, the challenge of visually discerning these alternans has hindered the creation of specialized annotated databases, consequently impeding the establishment of a gold standard for validating the efficacy of proposed methodologies. Consequently, from a clinical perspective, only two approaches have substantiated their validity by being utilized in multiple clinical investigations [40]. The **Spectral Method** (SM) [41] and the **Modified Moving Average Method** (MMA) [42]. In order to apply this methodologies, a few previous steps should be performed.

When examining TWA in surface ECG's, it's essential to focus on the ventricular repolarization segments of the ECG to identify a periodic pattern occurring every other beat. This involves encapsulating the set of N samples from the m-th ST-T complex into an N-dimensional vector:

$$x_m = [x_m(0), x_m(1), ..., x_m(N-1)]^T. \tag{2.1}$$

These repolarization segments are then organized row-wise into the M $\times$ N ma-

trix:

$$M = [x_0^T, x_1^T, ..., x_{M-1}^T] = [s_0, s_1, ..., s_{N-1}] \tag{2.2}$$

where each column represents M consecutive beats for analysis. The M $\times$ 1 vector $s_n = [s_n(0), s_n(1), ..., s_n(M-1)]^T$ contains the samples of M consecutive heartbeats collected simultaneously at the same latency n, forming a beat series. In surface ECG analysis for TWA, the signal is often obscured by high levels of noise and artifacts stemming from factors like physical activity or ambulatory recording. To ensure accurate interpretation, various preprocessing steps are employed, including linear filtering, baseline wander removal, QRS detection and delineation, beat alignment, and rejection. All this preprocessing steps will be better explained in deep in chapter 3.2. Matrix M in Equation 2.2 represents the result of several of these preprocessing stages. The design of these blocks involves considering different perspectives and employing diverse approaches [9].

Now that this previous steps are properly performed, the application of this methods can be assessed:

- **Spectral Method**: SM detects TWA in the frequency domain of the beat series, also known as the beat-frequency domain. This means that the inherent periodic pattern of 2, indicative of existing TWA, is observed as a component at 0.5 cycles/beat (representing repetition every two beats) in each column of matrix M. The SM calculates the power spectrum density function of each beat series using the periodogram equation 2.3:

$$P_n(f) = \frac{1}{M} \left| \sum_{m=0}^{M-1} s_n(m) \cdot e^{-j2\pi fm} \right|^2 \tag{2.3}$$

  for n = 0, 1, ..., N - 1. These spectra, computed at each point of the repolarization segment, are then averaged to consolidate the contribution of the entire ST-T segment into an aggregate spectrum.

$$P(f) = \frac{1}{N} \sum_{n=0}^{N-1} P_n(f) \tag{2.4}$$

  The K score, or TWA ratio, quantifies the magnitude of the power spectrum at the alternans frequency relative to the noise level:

$$K = \frac{P(0.5) - \mu_{\text{noise}}}{\sigma_{\text{noise}}} \tag{2.5}$$

  Where P(0.5) represents the value of the aggregate spectrum at 0.5 cycles/beat, and μ_{noise} and σ_{noise} denote the mean and standard deviation of the noise, respectively. The noise is estimated in a nearby reference band close to the

alternans frequency, typically around 0.4 cycles/beat. This idea can be fully understand by seeing the spectrum of the signals in figure 2.12 A K_{score} is considered statistically significant when the alternans component surpasses three times the noise level (i.e., $K > 3$).

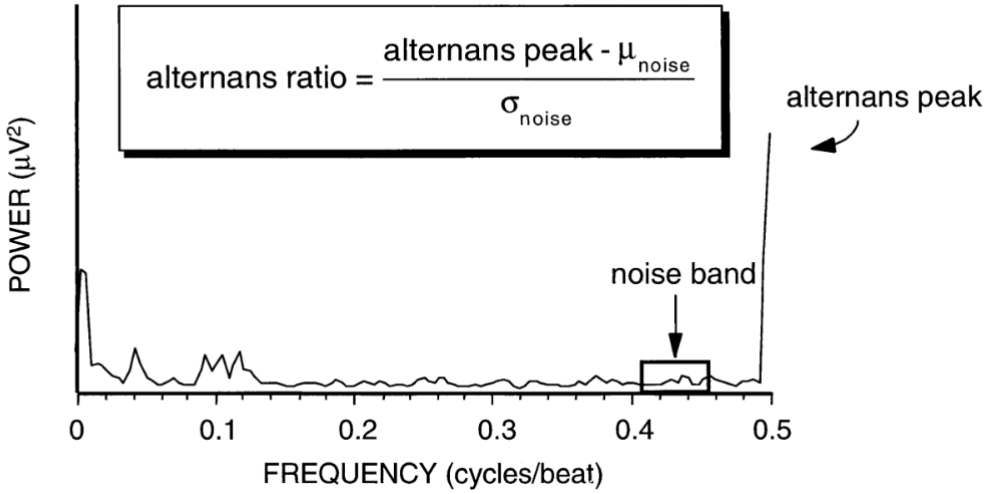

Figure 2.12: Representative example of power spectrum of beat-to-beat fluctuations in T-wave morphology [33].

The estimation of the alternant wave, V_{alt}, is determined as the square root of the difference between P(0.5) and μ_{noise} as in equation 2.6.

$$V_{\text{alt}} = \sqrt{P(0.5) - \mu_{\text{noise}}} \tag{2.6}$$

This signifies the average magnitude of the difference between the amplitude of even and odd beats compared to the mean beat.

Because the SM relies on spectral analysis, it necessitates quasi-stationary conditions over prolonged periods. Typically, a sufficient number of heartbeats, $M = 128$, is collected to obtain an aggregate spectrum. Simultaneously, during exercise, the patient is appropriately guided to elevate their heart rate within the valid range previously mentioned [9, 41].

- **Time Method (TM)**: The TM is going to estimate the TWA amplitude in a different way. Considering the matrix M already defined in equation 2.2, if we consider m_s^i the i^{th} row of M, considering that we have row-wise it; then the TM estimates the TWA amplitude as:

$$\text{V}_{alt} = \frac{1}{2}\left(\max\left|m_s^{\text{odd}} - m_s^{\text{even}}\right|\right) \tag{2.7}$$

where $m_s^{\text{odd}} = E_{iodd}(m_s^{\text{i}})$ and $m_s^{\text{even}} = E_{ieven}(m_s^{\text{i}})$ are the TWA templates for odd and even alternans, respectively, and E is the expected value, estimated as the sample average [22]. The TM and the SM previously explained have been used as features for the ML algorithms that will be seen chapter 2.4.

- **Modified Moving Average Method**: MMA approach presents a distinctive method that utilizes nonlinear averaging to estimate an alternant wave. Unlike

the Spectral Method (SM), which operates in the frequency domain, the MMA functions in the time domain, focusing on determining even and odd ST-T segment estimates separately as follows:

$$\hat{x}_m = \hat{x}_{\text{m-2}} + h_{\text{m-2}} \tag{2.8}$$

This is achieved through a recursive formula 2.8 where each estimate $\hat{x}_m$ is computed based on the previous two estimates $\hat{x}_{\text{m-2}}$ and a correcting factor $h_{\text{m-2}}$. The correcting factor $h_{\text{m-2}}$ is determined based on the error estimate e_{m} , which represents the difference between the actual sample x_m and the estimated sample $\hat{x}_m$.

$$e_{\text{m}} = \frac{x_m - \hat{x}_m}{8} \tag{2.9}$$

The MMA employs a nonlinear limit function to determine the value of h_{m}, which helps reduce noise and enhance the accuracy of the estimation process.

$$h_m(n) = \begin{cases} -32, & \text{si } e_m(n) \leq -32 \\ e_m(n), & \text{si } -32 < e_m(n) \leq -1 \\ -1, & \text{si } -1 < e_m(n) < 0 \\ 0, & \text{si } e_m(n) = 0 \\ 1, & \text{si } 0 < e_m(n) \leq 1 \\ e_m(n), & \text{si } 1 < e_m(n) \leq 32 \\ 32, & \text{si } e_m(n) > 32 \end{cases} \tag{2.10}$$

With this approach, an alternan wave measure is obtained as the difference between the estimates of even and odd beats. The TWA detection parameter, referred to as maximum alternans magnitude V_l, is then computed as the maximum absolute difference between consecutive estimates.

The MMA method offers advantages such as noise reduction and quicker reporting compared to the SM, making it suitable for applications like exercise testing where real-time monitoring is crucial. It also provides versatility in reporting TWA levels, allowing for potential use in ambulatory recordings to assess the risk of SCD. However, methodological studies comparing several methods have shown that the MMA may report false positive TWA due to the inherent T–wave variability, the influence of respiration in the ECG, as well as higher levels of noise and artifact contaminating the ECG, while others not [4, 43, 44] .While specific cutoff values for risk stratification have not been universally defined, certain thresholds such as $V_l > 60\mu V$ and $V_l > 47\mu V$ have been associated with higher SCD risk [9, 42, 45]. An schematic visualization of the method can be seen in figure 2.13.

Other methodologies have also been proposed by some authors for the detection of TWA. Among these ones we find the Correlation Method (CM), Poincaré Mapping Method (PM), Karhunwn-Loeve Transform (KLT), Capon Filtering (CF), etc. Nevertheless, for reasons of simplicity and since they are not used in this framework they will not be explained in deep.

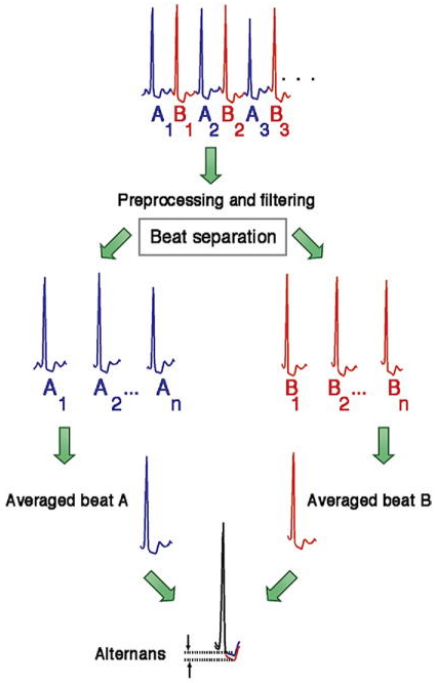

Figure 2.13: Flow chart of the major components of the Modified Moving Average (MMA) method of T-wave alternans (TWA) analysis [45].

2.4 Machine Learning

Machine learning (ML) is a field of artificial intelligence (AI) that focuses on the development of algorithms and statistical models that enable computers to learn and improve their performance on a specific task without being explicitly programmed. In essence, it allows computers to learn from data and make predictions or decisions based on that learning.

The impact of machine learning extends across a wide range of sectors and applications. In medicine, for example, it has facilitated significant advances in medical diagnosis, pattern recognition in medical images, diseases prevention...

This high impact has been translated in a skyrocketing growth of these techniques in thousand of works and researches throughout the world. Thus, ML algorithms and models can be considered the state of the art for certain applications and detection tasks.

ML is mainly composed by four main subgroups: **supervised** (see section 2.4.1), **unsupervised, semi-supervised, and reinforcement learning.**

Unsupervised learning (UL) is a fundamental branch of machine learning that deals with extracting meaningful insights and patterns from unlabeled data.

Unlike supervised learning (SL), where the algorithm learns from labeled examples, UL algorithms are tasked with discovering hidden structures and relationships within the data without explicit guidance. This approach is particularly useful in scenarios where labeled data may be scarce or expensive to obtain. UL encompasses various techniques such as **clustering**, **dimensionality reduction**, and **density estimation**, all aimed at uncovering the underlying structure of the data. By allowing algorithms to explore and analyze data independently, unsupervised learning plays a crucial role in tasks ranging from exploratory data analysis to anomaly detection and recommendation systems.

Semi-supervised Learning (SSL): SSL represents a form of ML that lies between supervised and unsupervised learning paradigms. In SSL, the dataset comprises both labeled and unlabeled data The primary aim of SSL is to address the limitations associated with both supervised and unsupervised learning approaches.

SL typically necessitates a substantial amount of labeled training data to effectively classify test data. However, this process can be costly and time-consuming. Conversely, UL operates without the need for labeled data, grouping data based on similarities through methods like clustering or maximum likelihood approaches. Nevertheless, a significant drawback of UL is its inability to accurately cluster unknown data.

To tackle these challenges, SSL has emerged within the research community. SSL offers the capability to learn from a small set of labeled training data and subsequently label unknown or test data. By leveraging a limited number of labeled patterns for training and treating the remaining patterns as test data, SSL constructs a model capable of effectively handling both labeled and unlabeled data [46].

Reinforcement learning (RL): RL is an interdisciplinary field within machine learning and optimal control that deals with how an intelligent agent should make decisions in a dynamic environment to maximize its cumulative reward. Thus, RL is a set of challenges in which an individual must learn to use feedback to work in a given context [47]. Unlike supervised learning, RL doesn't require labeled input/output pairs for training, nor does it need explicit correction for sub-optimal actions. Instead, RL focuses on striking a balance between exploring new options and exploiting existing knowledge to maximize long-term rewards, even when feedback may be incomplete or delayed.

2.4.1 Supervised Learning

Supervised learning is any ML approach where the model learns from already labeled data, making predictions or decisions based on input-output pairs provided during the training. There are four main steps in the development of a supervised

learning model. 1) Divide our dataset into training and test sets. 2) Use the training dataset to inform our model about the behaviour of the data. 3) Test our model using the test set to determine how well our model has learnt to differentiate the data. 4) Evaluate our model by means of different metrics.

There are two main tasks involving SL, regression, in which the variable to be predicted us usually numeric, and classification, in which a categorical variable is intended to be predicted.

In the realm of SL, there exists a multitude of algorithms, each with its unique strengths, applications, and underlying principles. Given the breadth and depth of this field, it's impractical to delve into every algorithm in detail within a single discussion. Thus, only some algorithms of interest for this work will be overviewed:

- **Logisitc regression**: Logistic regression is a Machine supervised parametric learning algorithm used for classification tasks. It is based on the concept of logistic function 2.11 to model the relation between the predicting variables and the target variable.

  The logistic function is defined as follows:

  $$f(z) = \frac{1}{1 + e^{-}z} \tag{2.11}$$

  where z is a linear combination of the predicting variables:

  $$z = \beta_0 + \beta_1 x_1 + \beta_2 x_2 + ... + \beta_n x_n \tag{2.12}$$

  where $x_1...x_n$ are the predicting features and $\beta_1...\beta_n$ are the calculated importance coefficients for each one. $f(z)$ is the estimated probability for each instance to belong to a certain class.

- **Decision Tree (DT)**: A non-parametric supervised learning method used for classification and regression. The objective is to create a model that predicts the value of a target variable by learning simple decision rules inferred from the data features. A very illustrative example is shown in figure 2.14.

  The fundamental idea behind a decision tree is to divide the dataset into smaller subsets while selecting features that best separate the classes of interest (nodes). This is done based on certain splitting criteria such as information gain or Gini impurity. A decision tree consists of nodes and edges. The root node represents the entire dataset, and from there, the tree branches out into decision nodes and leaf nodes. Decision nodes represent features of the dataset and decisions made based on these features, while leaf nodes represent the classes or output values. Additionally, decision trees can have a maximum depth, which limits the number of decision nodes and leaf nodes in the tree. This parameter helps prevent overfitting and controls the complexity of the tree.

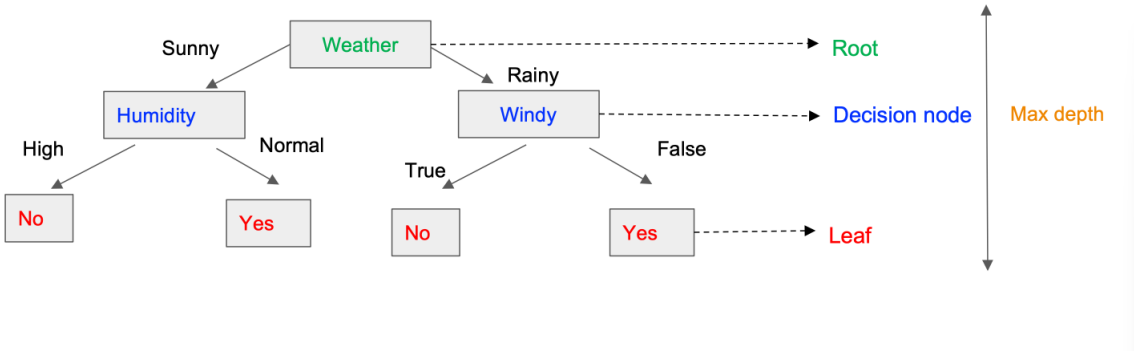

Figure 2.14: Decision tree example for the question Will I play tennis tomorrow?

- **Random Forest (RF)**: RF is a SL model which belongs to the ensemble methods. Ensemble methods combine the predictions of several base estimators built with the same training data in order to improve generalizability / robustness over a single estimator by introducing diversity. In the case of RF, the combine a group of DT to make their predictions. Each tree of the RF is trained with a random sample of the same dataset in a process known as bootstrapping or sampling with replacement.

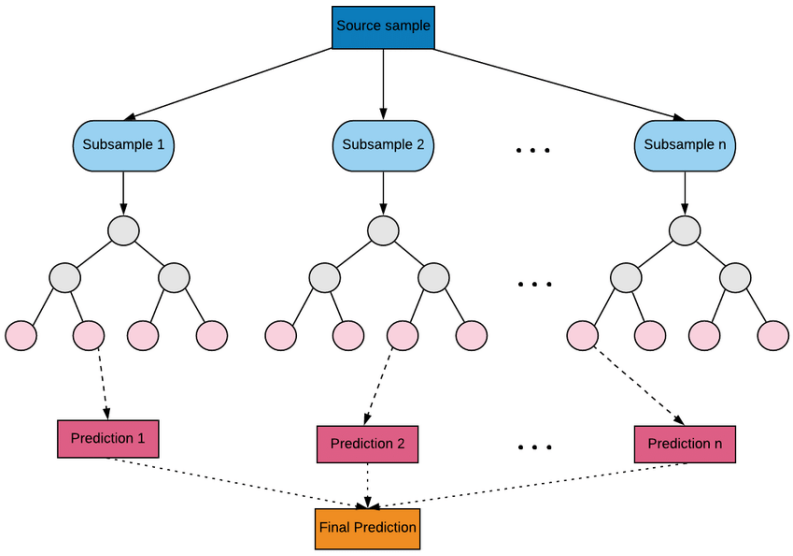

Figure 2.15: General structure of a random forest model [48].

The final prediction is determined by majority voting in the case of classification, or averaging the predictions of all the trees in the case of regression problems.

- **Support vector machine (SVM)**: SVM is a robust technique utilized for constructing classifiers. Its primary goal is to establish a decision boundary, referred to as a hyperplane, between two classes, facilitating the prediction of labels based on one or more feature vectors. This hyperplane is positioned to maximize the distance from the closest data points of each class, known as support vectors. Given a labeled training dataset: $(x_1, y_1), ..., (x_n, y_n), x_i R^d$

and $y_i(1, +1)$, where x_i represents a feature vector and y_i denotes the class label (negative or positive) of a training instance i. The optimal hyperplane is formulated as:

$$wx^T + b = 0 \tag{2.13}$$

where w represents the weight vector, x is the input feature vector, and b denotes the bias.

The values of w and b must satisfy the following conditions for all elements of the training set:

$$\begin{aligned} wx_i^\top + b \geq +1 \quad \text{if} \quad y_i = 1 \\ wx_i^\top + b \leq -1 \quad \text{if} \quad y_i = -1 \end{aligned} \tag{2.14}$$

The objective during SVM model training is to determine the values of w and b such that the hyperplane effectively separates the data while maximizing the margin, represented as $\frac{1}{\|w\|^2}$ [49].

A visual intuition of this algorithm can be visualized in figure 2.16:

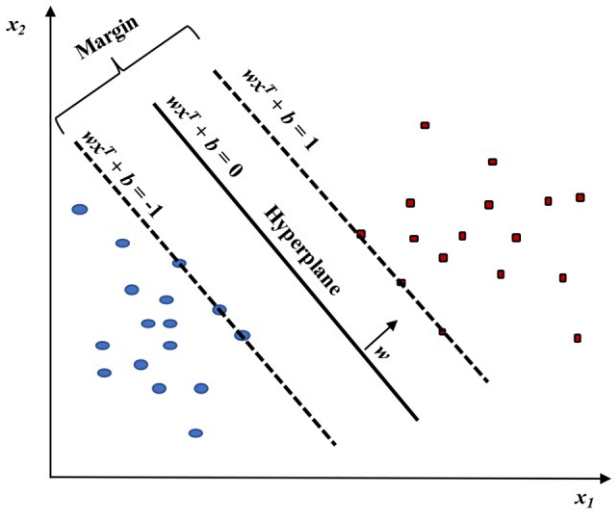

Figure 2.16: Linear SVM model. Two classes (red versus blue) were classified [49].

A problem that may arises from the SVM is that it was originally proposed for linear problems. An alternative application of SVM is the kernel method 2.17, which allows for the modeling of higher-dimensional, nonlinear relationships [50].

2.5 Deep Learning

Deep Learning (DL) is a branch of ML based on **artificial neural networks (ANN)** with multiple intermediate layers (hidden layers), focused on finding patterns in the data. An ANN is a mathematical model inspired by the biological behavior of neurons and the structure of the brain, used to solve a wide variety of

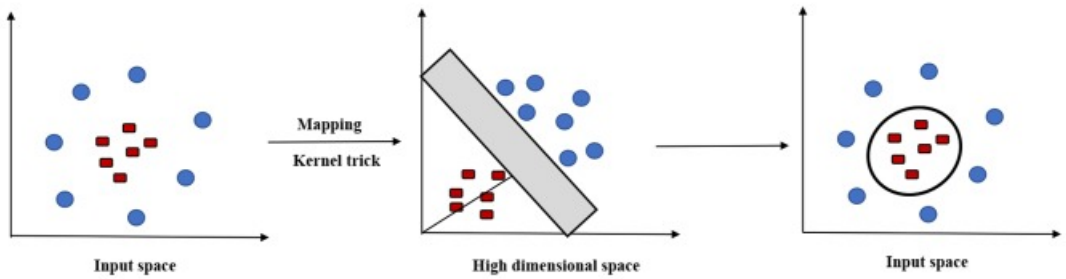

Figure 2.17: Kernel function. Data that cannot be separated by linear SVM can be transformed and separated by a kernel function [49].

problems. Due to its flexibility, a single neural network can perform various tasks. Just as in the structure of a biological neural system, the essential processing elements of an artificial neural system are neurons. An artificial neuron is a simple computational device that produces a single response or output based on a set of input data.

Neurons are grouped within the network forming layers. Depending on their position within the network, three types of layers are distinguished:

- **Input layer**: This layer directly receives information from the outside world and incorporates it into the network.
- **Hidden layers**: These are internal layers within the network responsible for processing the input data. We can have one or multiple hidden layers.
- **Output layer**: This layer transfers information from the network to the external environment.

The synaptic connections (the arrows entering or leaving a neuron) indicate the flow of signals through the network and are associated with corresponding synaptic weights as it can be seen in figure 2.18.

The main items visualized in figure 2.18 that compose a neural network are:

- **Set of inputs**: $x_1 \dots x_m$.
- **Synaptic weights**: $w_1 \dots w_m$.
- **Propagation rule** s that combines the inputs and synaptic weights. Usually:

$$s(x_1, ..., x_m, w_1, ..., w_m) = \sum_{i=1}^{m} w_i x_i \tag{2.15}$$

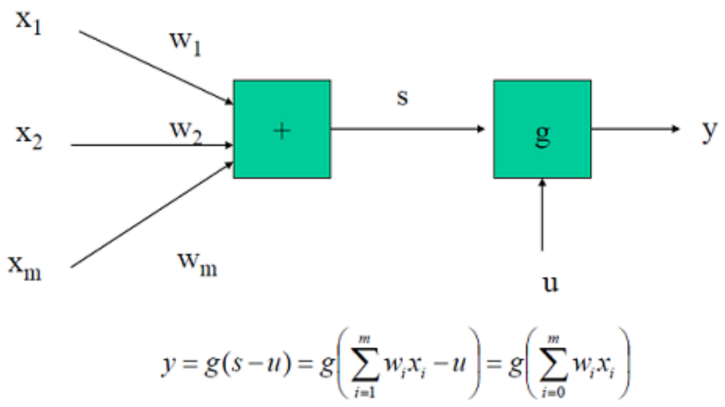

Figure 2.18: Artificial neural network scheme.

- **Activation function** g, which is a function of s and a constant u (referred to as threshold or bias), providing the output y of the neuron. Among the main activation functions we can find the logistic function, the hyperbolic tangent function, the ReLU activation function or the sigmoid function.

This concepts are key in the building of DL models. DL uses a cascade of multiple layers of nonlinear processing units (neurons) for feature extraction and transformation. The lower layers close to the data input learn simple features, while higher layers learn more complex features derived from lower layer features. The architecture forms a hierarchical and powerful feature representation. It means that DL is suited for analyzing and extracting useful knowledge from both large huge amounts of data and data collected from different sources.

But how do they learn and extract these features? The answer is the **backpropagation**. Backpropagation is a fundamental technique in training neural networks in the field of DL. This process is essential for adjusting the weights and biases of the neural network so that it can learn and improve in the specific task for which it has been designed. Essentially, training a neural network involves feeding input data through the network and comparing the outputs produced by the network with the desired outputs. The difference between these outputs is used to calculate the network's error. Backpropagation is responsible for propagating this error backward through the network, calculating the contribution of each weight and bias to the output error. This information is then used to adjust the weights and biases of the network so that the error is minimized.

The backpropagation process consists of two main stages: **forward propagation and backward propagation**. During forward propagation, input data is fed through the neural network layer by layer, and the outputs of each neuron are calculated using the current weights and biases. Once the network's outputs are obtained, the error is calculated by comparing these outputs with the desired outputs using a loss function [51].

Then, during backward propagation, the partial derivatives of the error with respect to each weight and bias in the network are calculated using the chain rule of calculus. These partial derivatives indicate how to change each weight and bias to reduce the output error. The weights and biases are updated using an optimization algorithm, such as gradient descent, which adjusts the values of the weights and biases in the direction that minimizes the error.

The backpropagation process is iteratively repeated throughout the training of the neural network, with the aim of gradually reducing the output error and improving the network's performance in the specific task for which it is designed [52].

There is a big variety of networks in DL; deep neural networks (DNN), deep belief networks (DBN), Generative Adversarial Networks (GAN), etc. However, in this project we will focus on **Convolutional neural networks and Recurrent Neural Networks.**

2.5.1 Convolutional neural networks

Convolutional neural networks (CNN) have become one of the most representative neural networks in the field of DL. CNN is a kind of feedforward neural network that is able to extract features from data with convolution structures. Different from the traditional feature extraction methods, CNN does not need to extract features manually [53, 54]. Goodfellow et al. [55] highlighted three main advantages

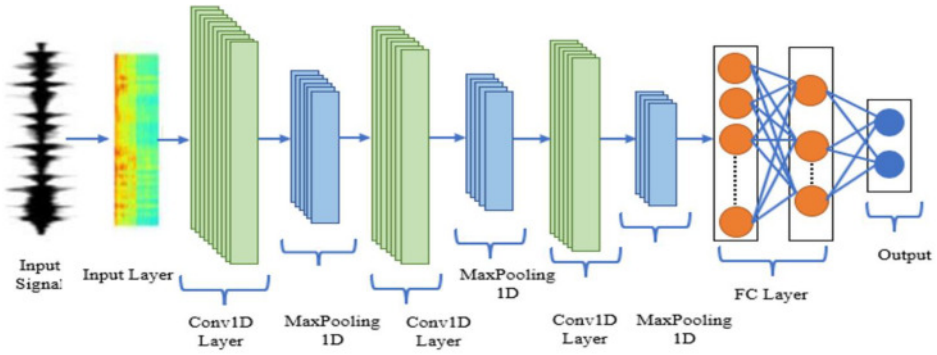

Figure 2.19: 1D-CNN general structure [56].

of Convolutional Neural Networks (CNNs): **equivalent representations, sparse interactions, and parameter sharing**. Unlike traditional fully connected networks, CNNs utilize shared weights and local connections to effectively process input data such as signals (1D) or images (2D). This approach significantly reduces the number of parameters needed, simplifying training and accelerating network performance. Analogous to the visual cortex cells, CNNs focus on small regions of input rather than the entire scene, spatially extracting local correlations similar to local filters.

This project, since the work is totally dedicated to signals analysis, will focus on 1D-CNN; 2D-CNN can be extrapolated from this explanation. A typical 1D CNN structure with its main components can be visualized in figure 2.19. In these structure the following layers can be defined:

- **Convolutional layer**: The key part of the CNN architecture lies in its convolutional layer, comprising **filters (kernels)** applied to the input sequence to yield feature maps. These kernels are arrays of numbers representing weights, initially randomized and then updated during training to capture pertinent features from the input [54]. During the convolutional process, the kernel convolves along the input sequence, computing dot products at each position to produce the output feature map. **Padding and stride** settings influence the output size, with padding playing a crucial role in preserving boundary information. A visual intuition of this process can be seen in figure 2.20.
- **Pooling layer**: The subsequent pooling layer follows the convolutional operations, downsampling feature maps to create compact representations while retaining key information. Various pooling techniques, such as max pooling and average pooling, can be employed.
- **Fully connected layer**: Typically situated at the conclusion of every 1D CNN architecture, the fully connected layer embodies a classic approach where each neuron interfaces with every neuron from the preceding layer. The input to the FC layer originates from the preceding pooling or convolutional layer. This input materializes as a vector, formulated from the feature maps subsequent to flattening. The output of the FC layer encapsulates the final output of the CNN.

Activation functions introduce non-linearity to 1D CNNs, enabling them to learn intricate patterns in sequential data. Common activation functions include sigmoid (used as final activation function in the final Dense layer in binary classification tasks), tanh, and ReLU, with ReLU being particularly favored due to its computational efficiency. However, while ReLU is popular, it can face issues like "Dying ReLU", where some neurons cease to activate, hampering the network's learning capacity. To address such shortcomings, alternatives such as Leaky ReLU have been explored, offering improved resilience against gradient saturation and vanishing gradient problems.

In addition to activation functions, the choice of loss function is crucial in training 1D CNNs. For binary classification tasks, the **binary cross-entropy loss function** is often employed. Binary cross-entropy measures the discrepancy between predicted probabilities and actual binary labels, guiding the network towards optimal parameter values during training. By minimizing the binary cross-entropy loss, the CNN learns to accurately classify sequential data, enhancing its predictive performance [54].

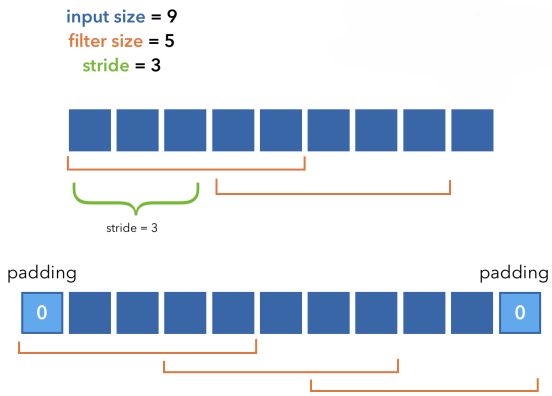

Figure 2.20: Padding, kernel and stride visual intuition. Top, a kernel of size 5 is applied to the input with stride of 3, resulting in two convolution steps but letting the last element without consideration. Bottom, padding is applied by adding 0's at both corners. This allows the filter to be applied in all the signal performing the convolution in three steps.

2.5.2 Recurrent neural networks

Recurrent neural network (RNN) is a specialized neural network with feedback connection for processing sequential data or time-series data in which the output obtained is fed back into it as input along with the new input at every time step. The feedback connection allows the neural network to remember the past data when processing the next output [57].

RNNs have been widely used for many application such as video analysis, image captioning, natural language processing (NLP), audio analysis or anything that involves a process over the time. There are a bast amount of networks that use these ideas for achieving different purposes. For reason of simplicity in this framework we will focus on the ones necessary for a complete understanding of the experimental part:

- **SimpleRNN (sRNN)**: sRNN architecture contains a simple neural network with a feedback connection. It has the capability to process sequential data of variable length due to the parameter sharing which generalizes the model to process sequences of variable length. Unlike feedforward neural networks which have separate weights for each input feature, RNN shares the same weights across several time steps. In RNN, the output of a present time step depends on the previous time steps and is obtained by the same update rule which is used to obtain the previous outputs.

  The RNN operates on an input sequence $x(t)$ with a time step index t ranging from 1 to τ, as illustrated in Figure 2.21. The time step index τ may not necessarily correspond to the passage of real-world time; it can instead indicate the position in the sequence. The cycles in the computational graph

depict the influence of past values of a variable on the current time step. The computational graph exhibits a repetitive structure that unfolds the recursive computation of the RNN, akin to a chain of events. It demonstrates the flow of information, both forward in time when computing the outputs and losses, and backward when computing the gradients [57–59].

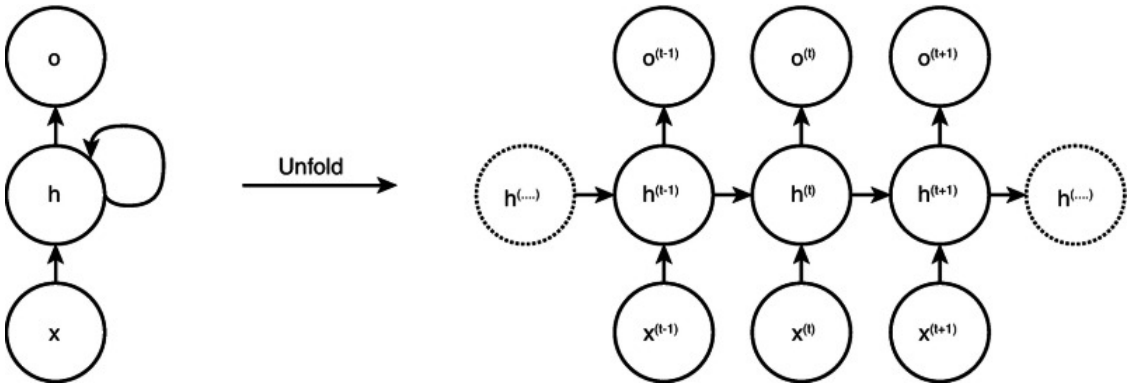

Figure 2.21: (Left) Circuit diagram for SimpleRNN with input x being incorporated into hidden state h with a feedback connection and an output o. (Right) The same SimpleRNN network shown as an unfolded computational graph with nodes at every time step [57].

The sRNN model performs adequately when handling short-term dependencies. However, when confronted with long-term dependencies, it struggles to retain the necessary information over extended sequences. This challenge arises primarily due to issues with gradient propagation, known as the **vanishing gradient** or exploding gradient problem [60]. As gradients are backpropagated through many layers, they often diminish to nearly zero or occasionally explode to excessively large values. This phenomenon occurs because the weight updates for long-term interactions are exponentially smaller compared to those for short-term interactions, making it challenging for the model to effectively capture and retain long-term dependencies.

- **Long short-term memory (LSTM)**: To address this long-term dependency problem LSTM were proposed. Thanks to the ability of these networks to remember long term dependencies LSTM have emerged as promising tools for time-series analysis applications. LSTM has an inner self loop in addition to the outer recurrence of the RNN. The gradients in the inner loop can flow for longer duration and are conditioned on the context rather than being fixed. In each cell, the input and output is the same as that of ordinary RNN but has a system of gating units to control the flow of information [60].

  In figure 2.22 we can see three gates. **The external input gate, the forget gate, and the output gate.** The forget gate at time t and state h^t decides which information should be removed from the cell state. The gate controls the self loop by setting the weight between 0 and 1 via a sigmoid function θ. When the value is near to 1, the information of the past is retained, and if the value is near to 0, the information is discarded. After the forget gate, the internal state i^t is updated. Computation for external input gate is similar to that of forget gate with a sigmoid function to obtain a value between 0 and 1

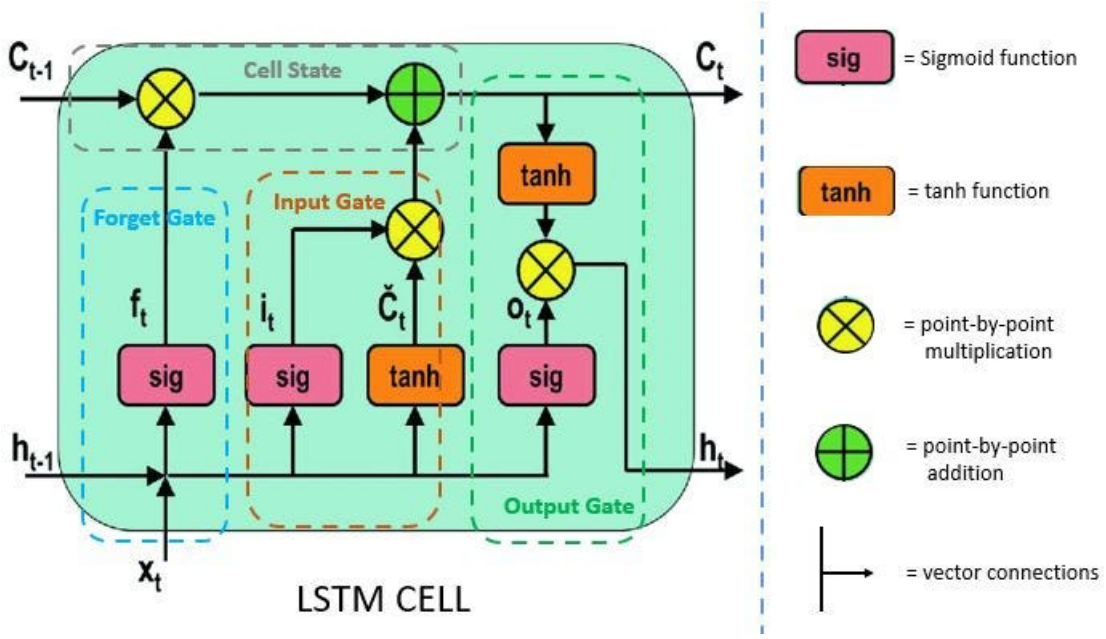

Figure 2.22: Long short-term memory with cell state c^t, forget state h^t, input i^t, and output o^t [57, 61].

but with its own parameters. The output gate of the LSTM also has a sigmoid unit which determines whether to output the value or to shut off the value h^t via the output gate.

The main advantage of using LSTM netoworks against the sRNN is the capacity of handling the vanishing gradient problem. The LSTM has the additive feature that they retain the past information by adding the relevant past information to the present state. This additive property makes it possible to remember a specific feature in the input for longer time. In SimpleRNN, the past information loses its relevance when new input is seen. In LSTM, any important feature is not overwritten by new information. Instead, it is added along with the new information.

2.5.3 CNN-LSTM networks

CNN-LSTM networks is an **hybrid DL model** that combines some of the beneficial characteristics of both the CNNs and the LSTM networks. A model 1D CNN-LSTM network can be over viewed in figure 2.23. The working procedure under these networks is divided into two main parts. Firstly, the **CNN performs a feature extraction** stage from the signals. These features will become the input for the second stage. This second stage is constituted by an **LSTM networks** which can capture the long-term dependencies of the input features sequences. This LSTM layers help in learning the temporal relationship between the features extracted in the convolutional stage. In other words, the main significant features of the signal are obtained in the convolutional stage, these features are supposed to have internal

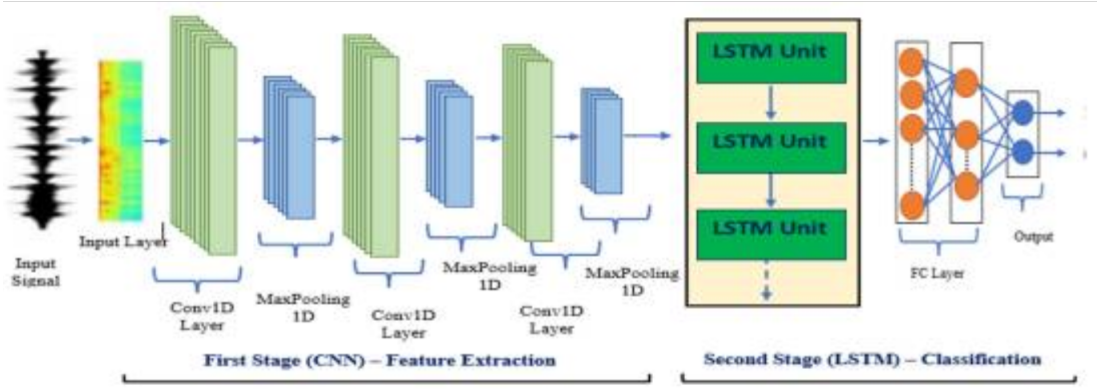

Figure 2.23: CNN-LSTM network model architecture [56].

temporal dependencies which are detected in the LSTM stage. After that usually a Dense layer is defined to interconnect all the results from the LSTM stage. Each of the stages have the same features previously explained in the above sections. In these framework a comparison between the performance of LSTM and CNN-LSTM networks for these concrete type of signals will be addressed.

2.5.4 Evaluation of models

In this section we will focus in the exploration of ways by which ML and DL models can be evaluated accurately. Evaluating ML and DL models is essential for ensuring their reliability, accuracy, and fairness. It helps assess performance, generalization ability, bias, robustness, and resilience. Additionally, it aids in model selection, comparison, iterative improvement, and promoting trust and transparency in AI systems.

One of the most common ways to evaluate models is the **K-fold cross validation**. In k-fold cross-validation, one divides the data D into k subsets of roughly equal size. The ML program is trained k times, each time leaving out one of the subsets from training, and using it for testing [62]. A visual intuition of this idea can be seen in figure 2.24.

In each iteration the performance on the test set is calculated depending on the metric of choice (explained later in these section), in order to evaluate the performance. Once the iterations finish, the metrics are averaged in order to have a global intuition on the model performance.

Therefore, from the K-fold cross validation two main values are obtained; the mean of each validation and the the global variance. The variance, in this sense, give us information regarding the stability and robustness of the model. Ideally, a perfect model would have low variance and high mean performance.

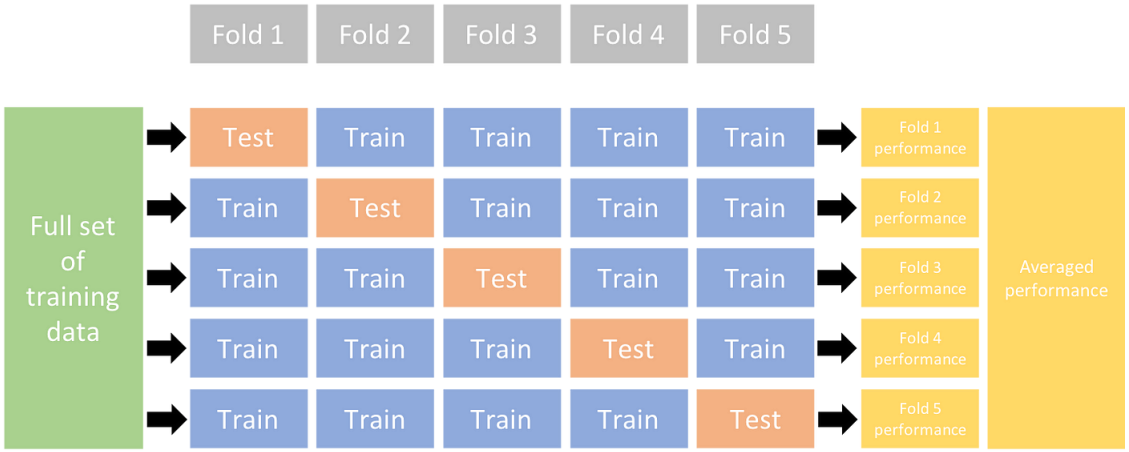

Figure 2.24: Performance accuracy estimation using a k-fold cross-validation method

Moroever, K-fold cross validation can be also used in the selection of hyperparameters. A **hyperparameter** is a parameter external to the model that has to be configured prior the training. The adjustment of them is so important as they are key in the training process. Adequate hyperparameters can lead to big changes in model performances. In this context, cross validation is useful, because allow us to select the best hyperparameters based on the performance obtained in the validation process.

A question that may arise now is how do we know the performance of our models?. In the ML and DL field there are various tools and metrics to evaluate the model performances. The adequate tools would depend on the task to be analyzed. In regression problems some common metrics would be the Mean Square Error (MSE), or the determination coefficient R^2. In clustering, techniques such as shilloutte analysis can be adequate.

In classification, the most common method is the **confusion matrix**. This matrix shows the relation between the models predicted values and the actual values of the classes as we can see in figure 2.25. It consists of four main regions:

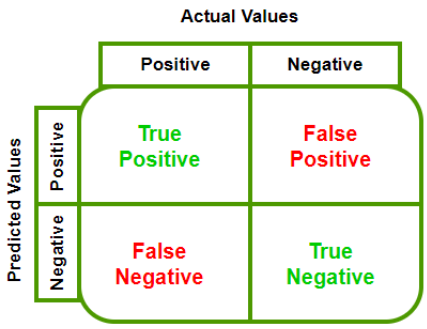

Figure 2.25: Confussion matrix

- **True Positives (TP)**: These are cases where the model correctly predicted an instance as belonging to a specific class when it actually does.
- **False Positives (FP)**: These represent cases where the model incorrectly predicted an instance as belonging to a specific class when it actually doesn't. In other words, the model predicted positive when it should have been negative.
- **False Negatives (FN)**: These are cases where the model incorrectly predicted an instance as not belonging to a specific class when it actually does. In other words, the model predicted negative when it should have been positive.
- **True Negatives (TN)**: These represent cases where the model correctly predicted an instance as not belonging to a specific class when it actually doesn't.

From these four values, several metrics can be obtained. Some of the most important ones are:

- **Accuracy**:
$$\text{Accuracy} = \frac{TP + TN}{TP + FP + FN + TN}$$
Accuracy measures the overall correctness of the model's predictions and is calculated as the ratio of correctly predicted instances (TP + TN) to the total number of instances (TP + FP + FN + TN).
- **Precision**:
$$\text{Precision} = \frac{TP}{TP + FP}$$
Precision measures the proportion of true positive predictions out of all positive predictions made by the model and is calculated as the ratio of true positives (TP) to the total positive predictions (TP + FP). Also know as positive predictive value (PPV).
- **Recall (Sensitivity)**:
$$\text{Recall} = \frac{TP}{TP + FN}$$
Recall, also known as sensitivity or true positive rate, measures the proportion of actual positive instances that were correctly predicted by the model and is calculated as the ratio of true positives (TP) to the total actual positives (TP + FN).
- **Specificity**:
$$\text{Specificity} = \frac{TN}{TN + FP}$$
Specificity measures the proportion of actual negative instances that were correctly predicted by the model and is calculated as the ratio of true negatives (TN) to the total actual negatives (TN + FP).

- **F1 Score**:

$$F1 = 2 \times \frac{\text{Precision} \times \text{Recall}}{\text{Precision} + \text{Recall}}$$

  The F1 score is the harmonic mean of precision and recall and provides a balanced measure of a model's performance.

These metrics provide valuable insights into different aspects of a model's performance, such as its ability to correctly classify instances, its sensitivity to positive instances, and its ability to avoid false positives. Choosing the most appropriate metric depends on the specific goals and requirements of the classification task at hand.

Another common way to evaluate the model performance is the **ROC curve**. The ROC curve is a graphical representation that show the relation between the TP rate (sensitivity) and the FN rate (1- specificity) for different decision thresholds.

A visual intuition of this metric can be seen in 2.26. The diagonal line (D) represents a random classifier while (A) would be a perfect classifier. The area under the curve (AUC), is a numeric metric that reviews the ROC, the higher the AUC the better the model is to discriminate between the classes.

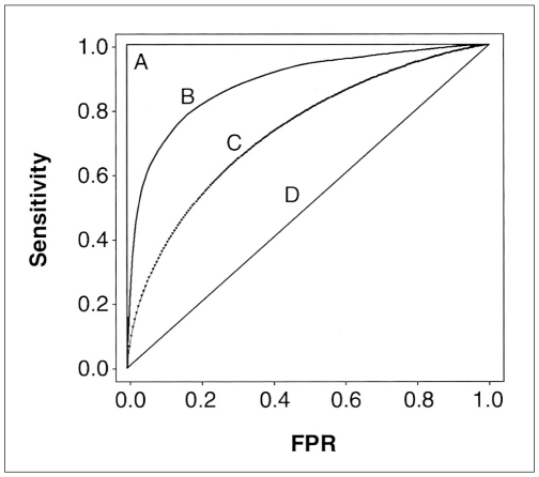

Figure 2.26: Four ROC curves with different values of the area under the ROC curve [63].

2.6 State of the art

In this section, we delve into the state-of-the-art advancements in TWA detection and analysis.

Two main methods have emerged as gold standard for the detection of TWA [64]. The SM [41] and the MMA method [65]. These methods have been tested in various clinical scenarios showing acceptable but still improvable results [66]. The importance of diminishing the SCD prevalence required from the improvement of the available methodologies [64]. In this scenario, some works appeared with the aim of combining the methodologies already proposed and tested for the TWA detection (SM, MMA, TM...) with the emerging ML technologies.

Under this novel framework idea, the work developed in [4] by Fernández-Calvillo et al. shed light on the TWA detection. This work compared different ML algorithms performance attending to different metrics using as features for the classifiers the results from the traditional methodologies. In that framework they decided to use the K-score from the SM, the V_{alt}^{TM} value from the TM and the V_{alt}^{MMA} from the MMA method. This work demonstrated the powerfullness of combining this attributes with the capability of finding hidden patterns in data from the ML algorithm.

As a result, an 88% accuracy was reported from the DT algorithm which is a big improvement compared to the the 79% accuracy of the SM alone which is considered to be the gold standard.

Other works in conferences were published under the same idea also reporting good results. In [67] and [68], a F1-score of 89% and 95.9% were obtained respectively.

Under this scenario, there is a crescent need of further research in the combination of traditional methods with the ML tools. Therefore, the experimental part of this project will try to evaluate ML algorithms with different features. At the same time it will try to dive into the application of DL methodologies which have shown great results in cardiac signals in different works.

With this project, thus, it is intended to improve the already obtained results giving rise to further advancements in the detection of TWA and as a direct consequence, the stratification of cardiac risk with a predetection of SCD.

Chapter 3

Data analysis

3.1 Data description

This section delves into the construction of the database and provides a comprehensive understanding of the data crucial for the project's development.

The primary challenge encountered at the outset of this project was the establishment of a suitable database for both ML and DL tasks. The complexity outlined in the background section, particularly concerning the detection of alternans, rendered the creation of adequately annotated databases containing real ECG data exhibiting alternans phenomena nearly impossible. To address this limitation, this endeavor adopted the approach elucidated by Fernández-Calvillo et al. [4], a methodology widely embraced across numerous studies [69–71].

Within this framework, a database optimized for ML purposes was constructed. In order to accomplish a faithful setting able to represent a realistic environment only real signals taken from ambulatory recordings were used. For this purpose, Physionet [72] is employed as the main source of ECG signals, since its open source nature ensures reproducibility.

Three public repositories from Physionet were used as sources of signals. Some signals were obtained from **MIT–BIH Arrhythmia Database (mitdb)** [73], others from the **European ST-T Database (edb)** [74] and the rest from the **MIT-BIH Normal Sinus Rhythm Database (nsrdb)** [73]. A signal would only be eligible to be part of this alternans ML-oriented database in the case 99% of its heartbeats are annotated as "normal". Moreover, the candidate signals also passed a SM test to rule out the existence of natural alternans on them. For further information on the amount of signals utilized from each database see Table 3.1.

For each of the signals the following storing format name is followed in order to have all the necessary information for posterior steps in the framework.

In other words, the storing format of the files contained:

- **Name of the repository**: an abbreviation representing the name of the specific database, providing a quick identifier for where the signal originates; edb, mitdb and nsrdb.
- **Patient id**: unique reference point to associate the signal with a particular individual's data. In further chapters it will be seen why the id of the patient is important for the ML algorithms.
- **ECG derivation**: ECG lead derivation is specified, indicating the specific lead or channel from which the signal was obtained
- **ECG segment**: name concludes with a designation of the segment of the ECG to which the signal corresponds.

An example of this database names would be: ***edb_106_l1_s1.mat***, where *edb* corresponds to the European ST-T Database , *106* is the patient id, *l1* is the lead and *s1* the first segment of the complete ECG signal. The storing format for each of the signals is .mat.

The complete set of 31 patients and their corresponding 574 signals is stored and used for the preprocessing stage that can be seen in the following chapter.

mitdb	**edb**	**nsrdb**
5 patients	14 patients	12 patients
13 signals	81 signals	480 signals

Table 3.1: Distribution of signals through the 3 databases

Each of the signals stored contained the following fields in order to have all the necessary information to correctly work with them: **Fs, ECG signal** and **QRS segment onset points.**

3.2 Data preprocessing

This section will cover all the necessary steps for the preprocessing of the signals which compound a crucial step for the analysis of TWA during the experimental section. The entire procedure was developed in the Python 3 programming language.

3.2.1 Alternans addition

At this stage it is needed to remember the lack of annotated databases involving ECG's with alternans. To solve this issue the alternans are added artificially to the signals which are free of any pathology. In order to have balanced classes in the future ML and DL algorithms it was decided to add alternans to half of the signals.

To do so, **12 different alternans waves were used**. The difference between these 12 signals is related to the shape of them. Randomly, these alternans waves were added to the signals to give more authenticity to the phenomena that appears in clinical scenarios. Moreover, these signals were resampled to meet the Fs from the different databases signals. This is; for the mitdb the Fs was established at 360Hz, for the edb at 250Hz and finally for the nsrdb at 128Hz. These signals waves were obtained from the work in [75] by J. P. Martínez et al.

The process of addition of alternans was developed in concordance with the work in [4]. Let's consider the ECG's as $p^{(i)}_{cont}(t), \quad t = 0, \ldots, L_i - 1$, where i denotes the i^{th} instance of the database and L_i its length. To obtain the ECG with alternans the following operation is performed on the ECG:

$$p^{(i)}_{alt}(t) = p^{(i)}_{cont}(t) + \sum_{k=1}^{N} g_k \cdot \epsilon(t - t_k - t_J) \tag{3.1}$$

where ϵ represents the alternan wave and L_ϵ their length which corresponds to the duration of the ST-T complex, much shorter than the whole signal length. In 3.1, N represents the number of heart beats (which in this framework is defined as $N = 32$), t_k is the starting time of the ST-T complex of the k^{th} beat. In order to add uncertainty a time delay t_J introduces a Jitter effect which is characterized as a zero mean Gaussian random variable with a standard deviation of 20 ms. Finally g_k represents the alternan amplitude, which alternates its value between 0 and α to represent the every–other–beat TWA fluctuation as stated in equation 3.2. In this framework different experiments will be carried out by varying the α value from 20 to 70 μV.

$$g_k = \begin{cases} \alpha, & \text{if } k \text{ is even} \\ 0, & \text{if } k \text{ is odd} \end{cases} \tag{3.2}$$

In figure 3.1, a comparison between a 3 seconds span time between the same signal with and without alternans can be seen. As expected both signals are overlapping which shows how impossible is to differentiate a TWA present ECG signal from a non-TWA present due to the μV nature of the waves. Therefore, further steps in the preprocessing will be required.

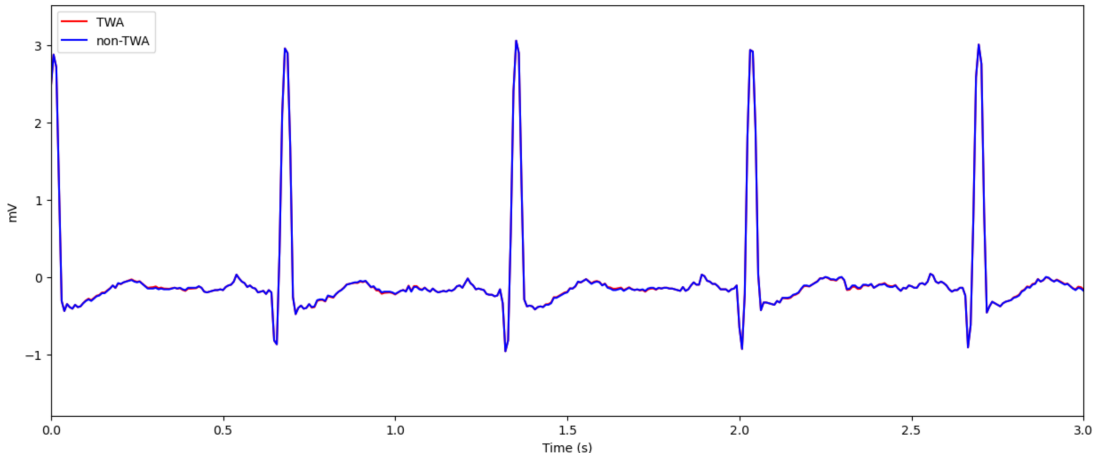

Figure 3.1: Comparison between TWA-signal with $30\mu V$ alternan amplitude(red) and non-TWA signal(blue).

3.2.2 Baseline wander removal

Baseline wander (BW) refers to the low-frequency oscillations or fluctuations observed in biological signals. BW in the ECG records produces artifacts data when measuring ECG parameters. These baseline interferences can be induced by electrode changes due to perspiration, movement and respiration. The frequency components of the BW are usually below 0.5 Hz but, in case of stress test, this limit can be higher. Thus, these components can be in the same range than the low frequency ECG components like those of ST segment altering the information contained in them making more difficult its analysis. [76].

In this project the methodology followed in [77], where the cubic splines method is shown to be the most effective approach for mitigating BW interference. In this work, **fiducial points** are used as reference markers for the ECG signals. Fiducial points are clearly-defined points in a normal ECG (for example the QRS complex or the T wave). This points are key in this process since they help to estimate adequately the baseline in order to remove it later. Therefore, once the fiducial points are defined, **cubic splines** were used to create a curve to them in order to estimate the BW. Once the BW is estimated the last step was to subtract the estimation from the original ECG. The result of this step can be seen in figure 3.2.

3.2.3 ST-T complex delineation

As said, the alternans were added in the ST-T wave of the ECG's. Thus, for a proper analysis it is intended to keep only the ST-T complexes from the signals.

The fiducial points (in this case the R wave) were used to determine the ST-T

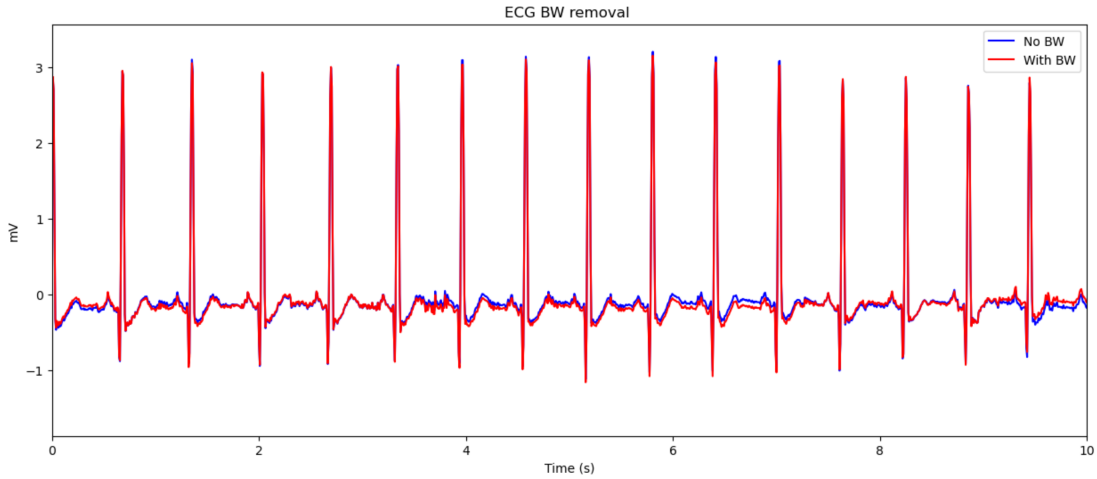

Figure 3.2: BW removal example

onset points. To do so, the distance between RR intervals is calculated and by predefining an standard ST-T interval duration as 300ms, the starting and ending points of the ST-T complexes were calculated.

Once we have that data the last step is to extract the ST-T complexes from the whole ECG and to store them in a matrix. Therefore, at this moment the structure of our data is represented in equation 3.3 where the rows n represent the data samples and the columns M represent the ST-T complexes to which the samples belong. The values of M and n depend on the Fs. A view of the result can be visualized in figure 3.3, where the difference in the amplitude of the ST-T complex can be appreciated between a signal with and without alterans in the even complex. The odd complex did not show this high difference in amplitude.

$$ST - T \text{ complex matrix} = \begin{bmatrix} ST_{1,1} & ST_{1,2} & \cdots & ST_{1,M} \\ ST_{2,1} & ST_{2,2} & \cdots & ST_{2,M} \\ \vdots & \vdots & \ddots & \vdots \\ ST_{n,1} & ST_{n,2} & \cdots & ST_{n,M} \end{bmatrix} \tag{3.3}$$

3.2.4 Heartbeat windowing

In this part of the preprocessing a segmentation of the ST-T complexes is performed in order to have a better tracking of the signals. The process works as follows: **a window of size** $M = 32$ **beats and step of** $m = 8$ **beats** slides over the ST-T complexes defined in the previous step. Each window will contain a set of ST-T complexes (exactly 32 ST-T complexes), the next window will contain the last 24 beats from the last window plus 8 new beats from the window step m.

Three main advantages are obtained from this process. Firstly, as alternans were

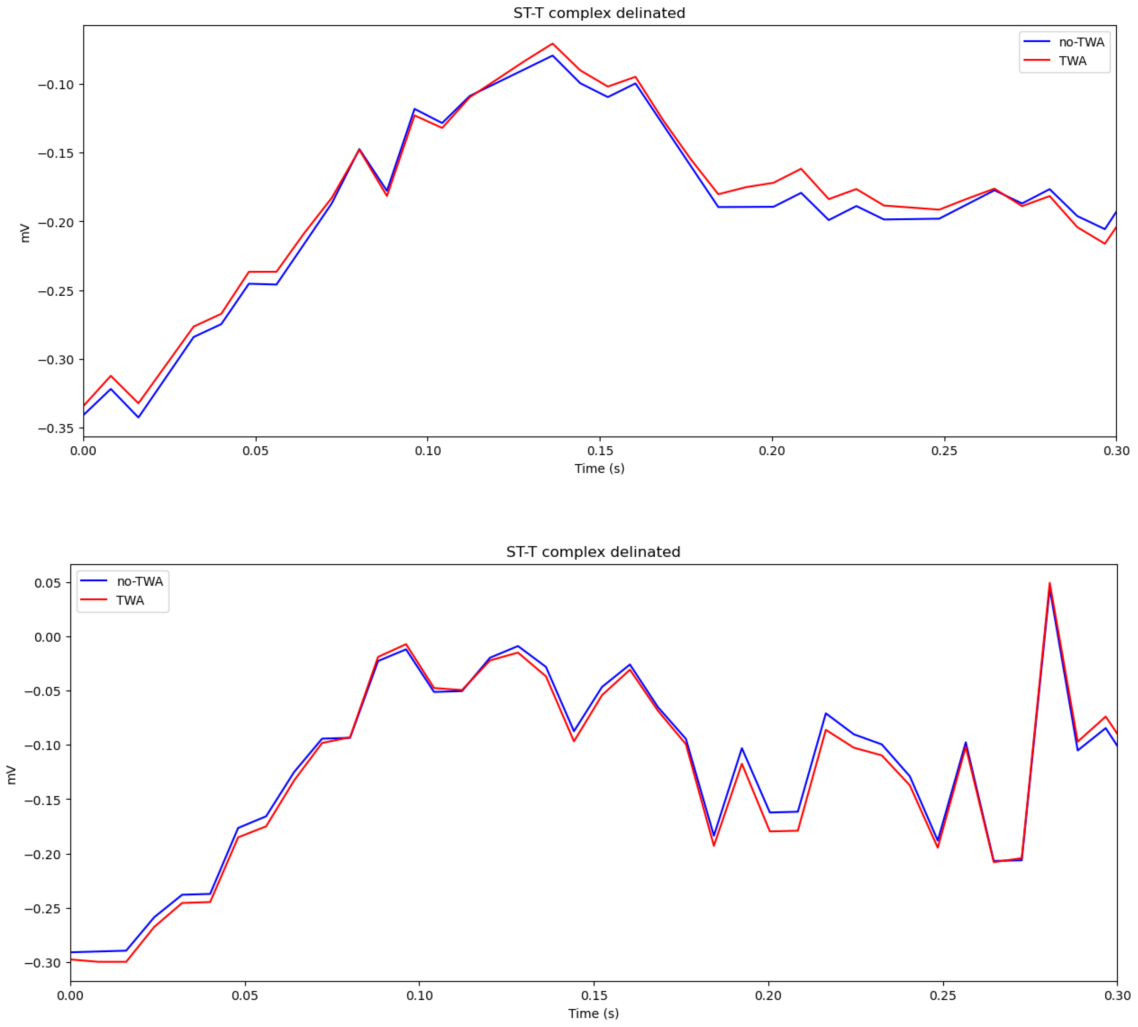

Figure 3.3: Even(Top) and odd (Bottom) ST-T complex of the same signal with and without TWA.

seen to be a transitory effect, the event can appear or not throughout the signal, and their effect can be blurred. Therefore, by dividing the long ST-T complexes into smaller windows makes easier the detection of TWA. Secondly, as we are creating multiple segments from a single signal we can treat each segment as a new instance, this is, we can increase the size of our dataset which is something really important in the development of ML and DL tools with reliability. Lastly, some methods from the feature extraction stage such as the SM requires from quasi-stationary signal conditions [4]. By sub-diving the signal into segments the chance of this algorithm to find alternans increases enormously.

Therefore, from this process the result would be a **matrix of dimensions** $[M, N, n]$, where M **indicates the window size** that in this case is 32 which internally denotes the number of ST-T complexes contained. N **corresponds to the number of samples that are contained on each ST-T complex**, and its value would depend on the Fs. Finally n **denotes the number of segments for**

each signal, which, as said, they will be treated as independent instances in the experimental section.

3.2.5 ST-T alignment

ST-T alignment is a usual procedure developed to correct the temporal deviation of ST-T complexes to ensure their correct alignment. The process works as follows:

1. A reference template of the ST-T complexes is calculated as the median of the ST-T complexes. Following a time window is established as it will determine the potential temporal variation of each complex from its starting location. This window is established to be the 3% of the Fs.

2. A portion of the echo signal encompassing the entire ST-T complex is acquired. Subsequently, these segments are time-stretched to synchronize the complexes temporally. The cross-correlation between the reference template and each time-stretched echo signal segment is then computed. This process aids in pinpointing the location of maximal similarity between the template and every time-stretched ECG segment.

3. Ultimately, the ST-T complexes are synchronized by determining the peak correlation point and utilizing it as the alignment reference for the corresponding ST-T complex.

The result of the difference between aligned ST-T complex can be seen in figure 3.4. It is also important to remark that the shape of the signal matrix remains as described in the previous step.

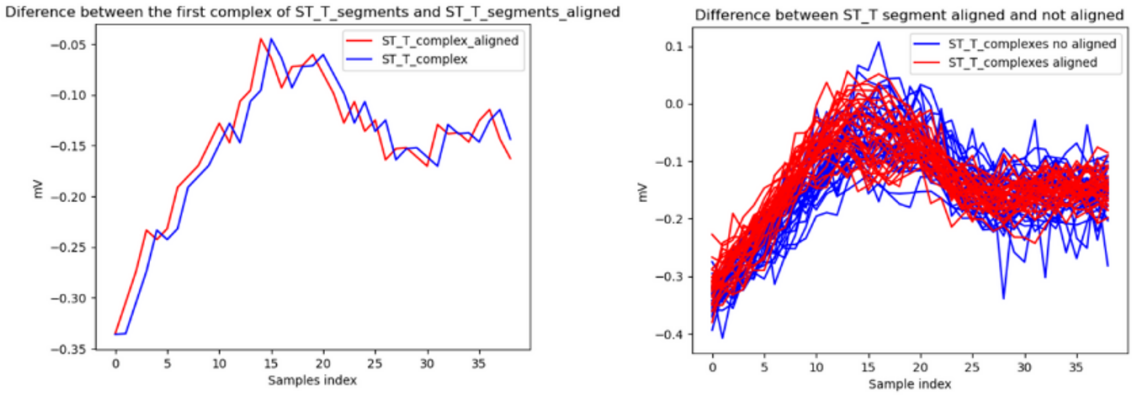

Figure 3.4: Difference between the 1st ST-T complex aligned and non-aligned(Left) and between all the complexes aligned and non-aligned of a segment (Right).

3.2.6 Background subtraction

This step in the preproceessing is the one focused in the isolation of the alterning component of the ST-T complexes in the case they exists (remember that only half of the signals contain it). Background subtraction is a method to remove an analogous underlying patterns that exists between successive ST-T complexes. In other words, subtract the ST-T complexes of two successive beats.

In this process a first pattern A of the signal is created, which contains the even beats of the ST-T segments. Then another pattern B is created which represents the odd beats of the ST-T segments. Finally, to ensure a correct alignment, a displaced version of A is created using a window (which in this case is 15 complexes).

Finally the A pattern is subtracted with the B pattern, and the displaced A pattern is subtracted from the B pattern. The result has the same dimensions as in the previous step. This process is executed all over the segments of the signal. The results of this process are shown in figure 3.5, as it can be seen the alterning components can be appreciated now as it has a higher amplitude, in other words, the subtraction between consecutive beats only got left the alterning component.

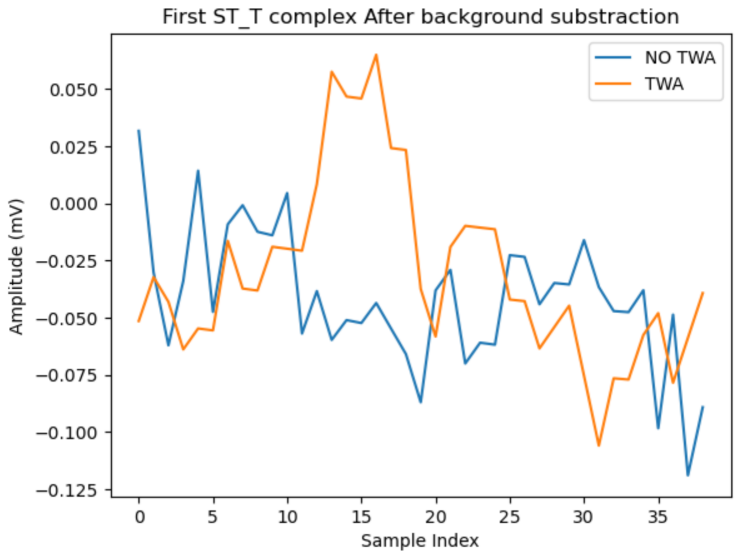

Figure 3.5: Comparison of first ST-T complex after background subtraction in the same signal with and without TWA.

3.2.7 Linear filtering

The final step in the preprocessing is the linear filtering. Linear filtering is a process by which undesired ranges of frequencies are removed. Since the alternating content is usually between 3 Hz and 15Hz, a band pass filter is going to be applied to all the ST-T complexes from all the segments.

To do this a FIR (finite impulse response) filter was applied with a Kaiser window using a value of β decided from kaiserord method [78]. To do so, a ripple attenuation and a stop-band attenuation were defined.

The result of this process together with a visual intuition of the Kaiser window can be visualized in 3.6.

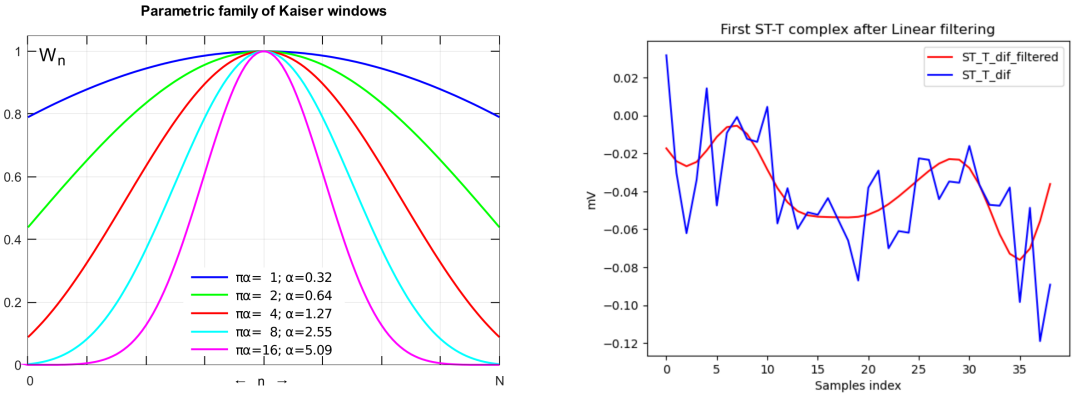

Figure 3.6: Kaiser window for different α values (Left). Result of applying it to the first ST-T complex (Right)

3.2.8 Signals dataframe building

The last step in the preprocessing is the construction of a new dataframe (DF). As said in the previous steps, as a result of the windowing of the signals, several segments were obtained from each of the signals. From now on, these segments will be treated as independent signals. This is, in other words, that our dataset dimensions goes from 574 signals to **136488 segments/signals**. This step differs from the work developed in [4], in that work only 25 segments per patient were used in order to have the same number of segments for every patient with a purpose of balancing the data. In this work we have considered more beneficial to work with the entire set of signals although some bias may be introduced. This process is helpful specially for increasing the amount of data to train the ML and DL algorithms, which is a necessary steps in order to increase the reliability and robustness of them.

Apart from the segments, other attributes for each segment are also stored:

- **Patient id**: The id of the patients constitutes a very important attribute in this framework. In ML, one crucial consideration is how we split the data into training and testing sets. Specifically, when dealing with segments of data corresponding to individual patients, it's imperative to either include all segments from the same patient in the training set or the testing set, but not mix them between the two. The rationale behind this practice is to prevent the algorithm from inadvertently learning patient-specific features rather

than general patterns within the signals. By segregating the segments of the same patient into either the training or testing set, we ensure that the model learns to generalize across various patients rather than memorizing idiosyncratic characteristics of individual subjects. Mixing segments from the same patient across both training and testing can lead to overfitting on the training data and poor generalization performance on unseen data.

- **Sampling frequency (Fs)**: The Fs is also an important factor to take into account. As said in section 3.1, the signals are coming from 3 different databases, and thus, they have been sampled at different frequencies. For some feature analysis of the signals, these values of Fs for each specific signal are necessary.

- **Label**: Finally, since our algorithms will be from the SL part, there is a necessity to store a value representing if the signal contains or do not contain an alterning component. In this framework it was decided that **"0" represents no TWA, and "1" represents yes TWA.**

- **Alternan amplitude**: The TWA amplitude used in the alternans addition step for each of the signal was also stored. This values are ranging from 20 to 70 μV randomly.

Chapter 4

Experiments

4.1 Feature extraction and selection

In the ML field, **feature extraction** constitutes a fundamental process that looks for the identification of relevant variables related to a certain dataset. This variables, usually named as features are the elements used by the algorithms to learn patterns and make accurate predictions [79].

Under this context, this section tries to define features of interest to feed our ML algorithms.

- K_{score} **index**: As it was seen in chapter 2.3.4, the SM constitutes the gold standard method in the detection of TWA. In order to use this value as a feature it was decided to apply the SM to the preprocessed signals (as a remember, from now on it is consider each segment obtained in the preprocessing stage as our signals, which is composed of 32 ST-T complexes differences). Originally the SM predicts that a signal contains TWA if the $K_{score} > 3$; otherwise it considers that the signal is not containing TWA. In our case, the concrete value of the K_{score} obtained from the SM was used as a feature.

  To do so, the **power spectral density (PSD)** for each signal was calculated. A **very important remark** needs to be done here: Let's consider the signal as a big matrix where the rows define the ST-T complex difference and the columns the samples for each ST-T complex difference. If the PSD in rows was computed (by calculating the PSD of the ST-T complexes difference), the result would not have a repetitive pattern. Therefore, the PSD is calculated in columns. The reasoning behind this is that by evaluating it in columns the spectrum of the **same electric cardiac moment over a series of beats** is obtained, and there is where a pattern every 2 beats may be found. That

retake, in fact, the idea of looking at the 0.5 frequency of the spectrum.

Once each PSD was calculated they were averaged to get a common feature for each signal. Once this was done the K_{score} was calculated according to the formulas seen in previous chapters. A visual intuition of the comparison between the averaged PSD of a TWA signal and a non-TWA signal can be seen in figure 4.1 where a clear difference in the $P(0.5)$ can be seen. It is important to remark that not every signal in the dataset show this clearly differentiated behaviour.

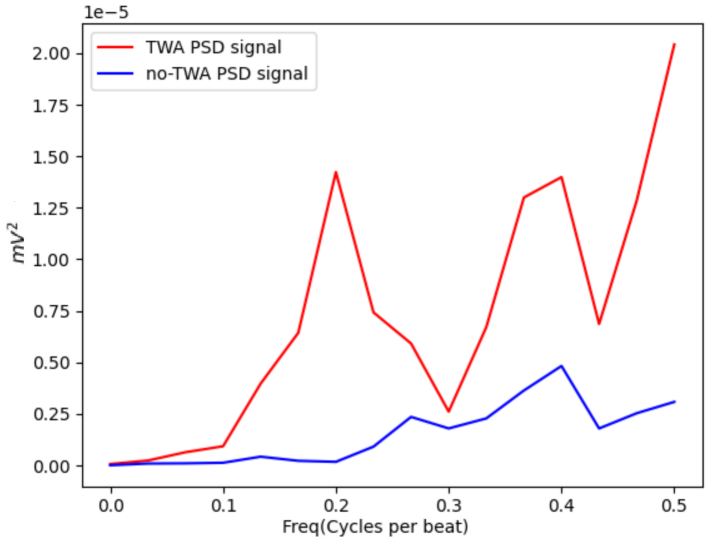

Figure 4.1: Average PSD calculated for a TWA signal (red) and a non TWA signal (blue).The K_{score} obtained were 4.45 and 0.26 respectively.

- V_{alt}^{TM} **index**: The TM was also used to obtain a feature. Following the same procedure as with the K_{score}, the TM was applied to every signal obtaining an index. This index will be used as a new feature.

These features were used together with the MMA method index in [4]. In this work, MMA was not used to create new features based on the works developed in [43] and [44] where it is shown that MMA tends to report false positive TWA. From now on, the features used are a nobel approach in order to find other variables that may increase the accuracy from the ML algorithms.

- **Cumulative sum detection change (CUSUM)**: The Cumulative sum test has been proposed to detect systematic changes over time. It has been shown to have the ability to detect unusual patterns [80]. It has been successfully used in fault detection, onset detection in seismic signal processing, and detection of changes in mechanical systems [81].

  In this framework, the CUSUM test was used in order to detect big changes in the power spectrum value from the PSD (calculated using the hamming

window) of the signals near 0.5 Hz. As it was seen, the $P(0.5)$ is a representative feature for TWA detection theoretically. However, in the real signals it was seen by visual inspection and trials that many non-TWA signals exhibit a high K_{score} value resulted from a very low θ_{noise}. This relationship was stated in equation 2.5, and it can be seen how as θ_{noise} is in the denominator, small values of it can increase erroneously the value of the K_{score} although they do not exhibit an alterning component. This behaviour can be seen in figure 4.2. In other words, these signals were meant to have a high probability of being detected as TWA-signals because of a generalized low value of θ_{noise} and not for having a big difference in the frequential component between the frequencies below 0.5 Hz and 0.5 Hz.

This technique, therefore, tries to differentiate TWA signals and non-TWA signals based on a big change in the value between the power in 0.5 Hz and the immediate value before 0.5 Hz. To do so, the following procedure was followed. Firstly, the average PSD was calculated together with the mean value of that PSD. Then, the CUSUM value from the signal centered on the mean value calculated is performed. Secondly, a threshold established at $1.96\times$ θ_{PSD}, where θ_{PSD} represents the standard deviation of the average PSD, was calculated. This threshold is used as the criterion to detect significant changes in the signal. Finally, those signal points where the cusum value is higher than the threshold were defined as significant signal changes samples.

In the case a change point was detected in the point corresponding to $P(0.5)$, the signal were marked as 1, otherwise they were marked as 0. This created a new feature for each signal, concretely a **categorical feature**.

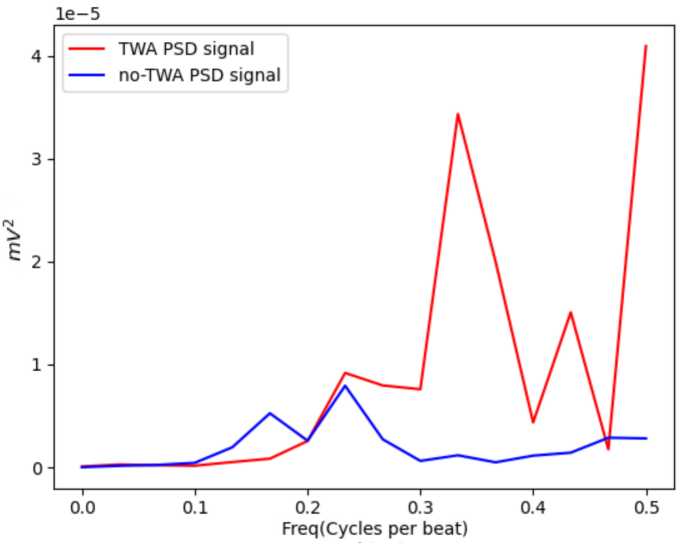

Figure 4.2: TWA signal (red) and non-TWA signal (blue). The K_{score} in each signal was 7.35 and 18.79 respectively. We can see that while a small change in the previous part of the non-TWA signal is seen, in the TWA signal a big change in the previous signal sample is appreciated. With the CUSUM test each signal would be detected as 1 and 0 respectively differentiating them appropriately while with the SM both signals would have been identified as containing alternans.

- **Root mean square (RMS) and standard deviation (STD):** Also the

RMS and STD of the signals in the time domain were calculated. To do so, the STD and RMS for each complex was obtained and then averaged to get a final value of STD and RMS to be used as features. Higher STD and RMS values are expected to be in the TWA signals.

- **Peak frequency**: This feature tries to look for the value of the PSD as the exact 0.5 frequency component. Ideally, the TWA signals would have higher values while non-TWA would have lower values.

Once these features were obtained for all the signals, **feature selection algorithms and correlation analysis** were used to test whether the features have a significant relationship with the outputs and whether they are helpful to achieve better results. For further clarification on this part, in section 7.1 from the Annex there are some interesting figures to consult.

1. **Variance thresholding**: Variance thresholding is a technique used in data preprocessing for feature selection. It involves removing features from a dataset that have variance below a certain threshold. The variance of a feature measures how much the values in that feature vary from the mean. Features with low variance indicate that the values within that feature are mostly similar or constant, which may not provide much useful information for modeling. This technique was used in order to know which continuous features were useful for the ML algorithms. The results from this feature selection mechanisms can be seen in figure 7.1. As it can be observed the variance thresholding stated that the most useful features were by far the K-score and the V_{alt}.

2. **Chi-squared test**: The chi-square test measures the independence between categorical variables and the target variable. It assesses whether there is a significant association between a categorical feature and the target, based on the observed and expected frequencies of their joint occurrences. This feature selection mechanisms was used in order to know if the CUSUM feature (which is categorical) was giving predictive information. The chi-square test showed that also the CUSUM was giving important information based on a high chi-square value obtained together with a almost null $p - value$ showing the high significance of this result. This results can be seen in figure 7.2

3. **Correlational analysis**: In order to examine the relations between features in a dataset, the correlational matrix constitutes a powerful tool. In this framework, the Pearson correlational matrix was used where -1 and 1 indicates highly correlated features and 0 no correlated futures. With this analysis it is intended to keep only the features with no correlation between them in order to reduce redundancy. In figure 7.3, the relations between features can be observed. It can be seen a high relation between the RMS and the STD, together with a high relation of the K-score, V_{alt} and CUSUM with the output. Finally a high relation between the peak and the V_{alt} is appreciated which may lead to not considering the peak as an adding information feature.

Thanks to the application of these feature selection algorithms, it was decided to use as final dataset for the ML algorithms a data frame composed of the K_{score}, V_{alt} and CUSUM features, together with the respective label. In figure 4.3, the distribution of the values of these three features for 1000 signals is represented. As it can be seen, just by visual inspection a "correct division of the data" is obtained.

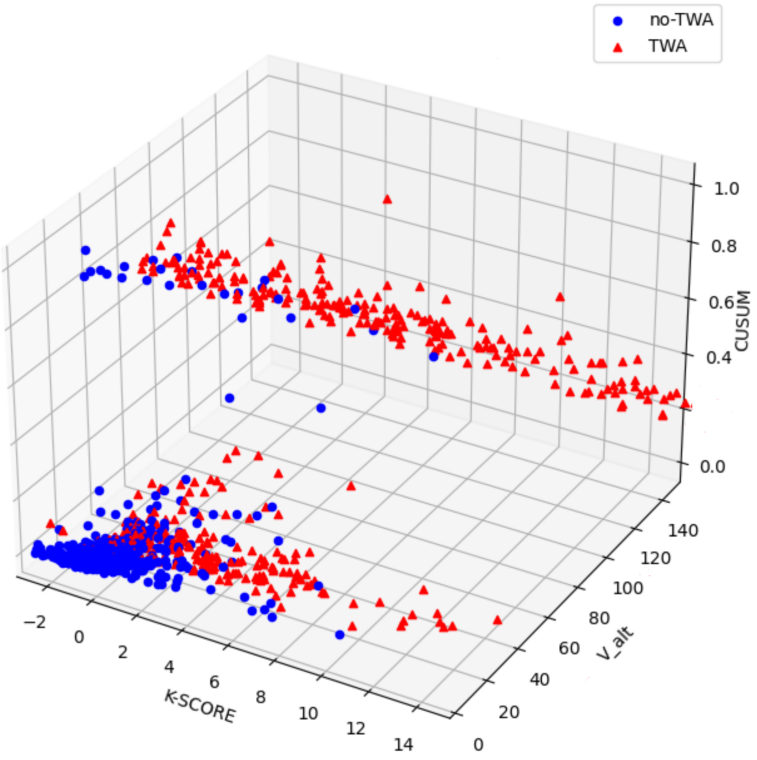

Figure 4.3: Input features (K_{score}, V_{alt} and CUSUM) 3D plane with the values for 1000 signals for these three features. In blue the non-TWA signals and in red, the TWA signals ($30\mu V$ amplitude).

4.2 Machine Learning algorithms

Once the dataset with the features is correctly defined, the next goal is to feed the ML algorithms with data to make the predictions.

The first step in this procedure is the subdivision of the dataset in two subsets; the **training set** and the **test set**. As it was discussed before, an important aspect to take into account in this subdivision is to make sure that every segment corresponding to a patient is stored in the training set or in the test set but not mixed. Following this procedure, a self-created train-test split function was used using a 0.3 splitting ratio. Therefore, the training set would be composed of around 105000 signals while the test set is composed of approximately 35000 signals.

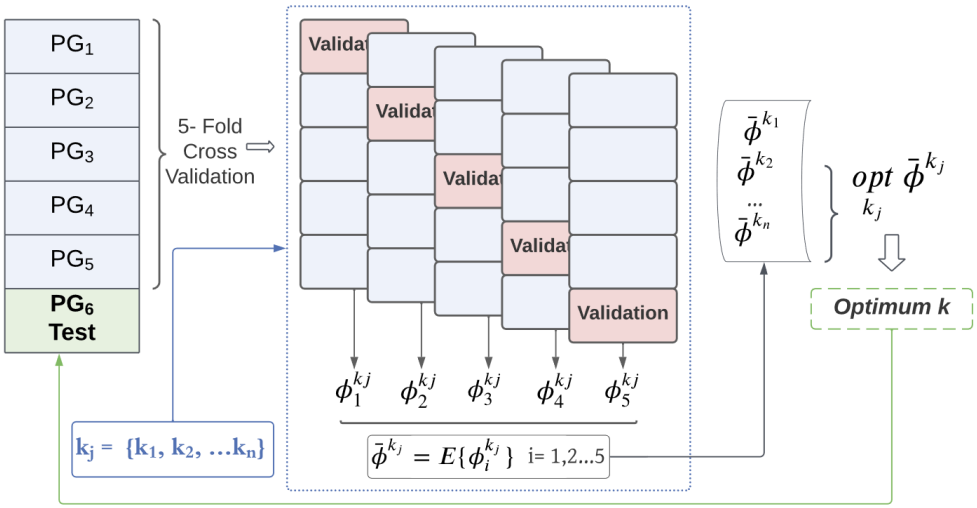

Figure 4.4: Cross Validation scheme of a model, where PG stands for Patient Group, k_j refers to the hyperparameters tuple of a model, and ϕ stands for the metric utilized for the optimization problem. Patient group test set (PG6) is fitted with optimum hyperparameters obtained from CV. Notice that each PG corresponds to a disjoint group of patients [4].

Once this two sets were created, the scikit learn python library [82] was used in the creation of the ML algorithms. Four main algorithms were developed in this project: **Logistic regression, decision tree, random forest and support vector machine.**

For each of these algorithms, a **Five-fold CV** is performed for hyperparameter tunning. It is important to remark that this subdivision between training and validation follows the same splitting procedure as the training and test set division. To do so, hyperparameter search using 5-fold cross-validation, conducted across patients from groups 1 to 5 (PG1-PG5), with each fold corresponding to a distinct group of patients. In this cross-validation setup, the model's performance is assessed for the j-th hyperparameter tuple $k_j = \{k_{j1}, k_{j2}, \ldots, k_{jl}\}$, resulting in metrics $\phi_i^{k_j}, i = 1, \ldots, 5$ obtained from the validation set of each fold, subsequently averaged across the five folds. A representative scheme of this procedure can be seen in figure 4.4. In this project, as the distribution of classes is balanced (46.91% of training signals corresponding to no TWA and 53.08% 4.5) it was decided to use **accuracy** as metric for the optimization procedure. As a final remark two experiments in each of the ML algorithms were performed. One experiment will correspond to the entire signal dataset with a T**WA amplitude of 30**μV. In the other experiment it was decided to use as amplitudes for the **TWA random values ranging from 20 to 70** μV. This second experiment is performed in order to test the capability of the models to distinguish alternans at different amplitudes which would mean an added robustness. In figure 4.6, the distribution of the alternans amplitude by μV intervals over the training and the test set can be observed, showing a more or less uniform distribution over the two sets of samples.

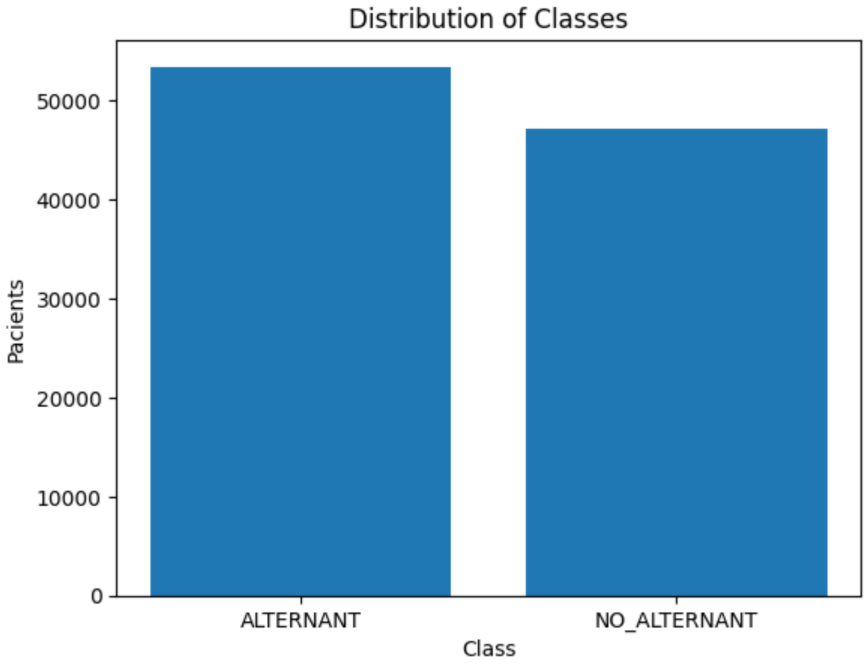

Figure 4.5: Distribution of classes in the training set.

4.3 Deep Learning algorithms

For this section, the entire signals will be used instead of obtaining features from the signals. Before entering in the DL networks used in this project a couple of preprocessing stages were necessary as two main problems appeared. Firstly, as the Fs of the signals were different (128, 250 and 360Hz), the number of samples on each of the complexes on each segment is also different. Secondly, the previous structure of the data frame used in the ML section has sinless applied to DL, thus, a new structure must be created to take the advantage of the characteristics of the networks.

The first problem is solved by applying a **sub-sampling of the signals to 128Hz**. Sub-sampling, in the context of signal processing, refers to the process of reducing the number of samples in a signal by selecting a subset of the original samples. As seen in table 3.1, the majority of signals corresponds to the nsrdb group, sampled at 128Hz. As sampling techniques may affect the quality of the signals it was decided to apply this procedure to the less number of signals possible. Therefore all the signals belonging to edb and mitdb databases were sub-sampled to 128Hz.

The second problem is solved taking into account the characteristics of the LSTM networks that will be used in this experimental section. As LSTM networks are meant to remember long term dependencies in time-series, the following data structure was built. Each of signals in the original dataset had the following structure resulting from the pre-processing stage: $[M, N, n]$. n denoted the number of segments

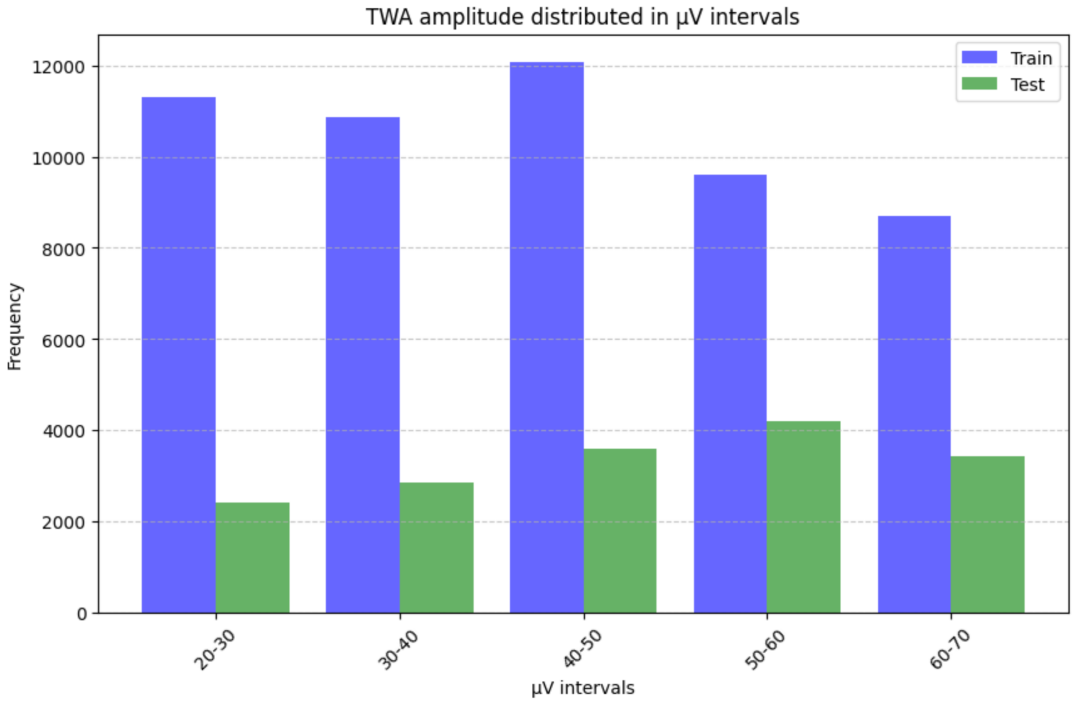

Figure 4.6: Distribution of alternans amplitude in μV intervals over the training (blue) and the test (green) sets.

for each patient, and as said each of the segments will be treated as independent signals. N denoted the number of samples in each signal complex, which as said previously, they had been sub-sampled to have the same structure in each segment. M, denoted the number of complexes contained. With this structure again in mind, each instance of the data frame will be composed of $M = 32$ columns, each of them composed of an array of $N = 39$ samples each. Therefore, each instance of the data frame will have all the entire signal recorded and preprocessed as a **complete long signal time-line**, which is expected to obtain the best performance based on the characteristics of the LSTM networks. The dimensions n represents, at the end, the number of signals from the same patient that are present in the dataframe, being the only value that varies according to the patient. Finally, the data was subdivided in three main sets; training, test and validation set, with 91255, 35899 and 9334 signals respectively. The disjoint rules previously mentioned were followed.

Once these two problems were faced and solved, the construction of the **LSTM and CNN-LSTM networks** architectures was developed.

A question that may arise now is **why are LSTM and CNN-LSTM seen as a possibility to improve the already obtained performances in previous works?** In this framework, in consonance with other works where ECG signals are analyzed using LSTM networks and CNN-LSTM networks for different purposes like AF detection [83], myocardial infarction detection [84] or QRS complex detection in noisy ECG's [85], it is expected that the signals, which at the end are a temporal line of points have some kind of temporal dependency within each others and this

temporal dependency can be caught by the LSTM layers of these networks. As we have seen each input of the network is of the shape $[32, 39]$. This makes probable that between the 32 signal vectors there are contained dependencies which are not identified neither by the traditional detection methodologies nor the ML algorithms. From the other side, trials on the CNN-LSTM will be also performed to test whether the previous acquisition of features by the CNN layers give more information to the LSTM layers than just the signals by themselves.

For each of the networks, experimental structures were built with the help of the **keras python library**, [86] and the **tensorflow python library** , [87].

The **architecture of the LSTM network** has the following parts:

- **LSTM layers:** The network starts with four LSTM layers, each with a progressive decrease in the number of units. Each layer had 256, 128, 64 and 32 units respectively, and a *Dropout* of the 20% in order to reduce overfitting. For each of the layers a ReLU activation function was used. Finally, the return sequences option in each of the LSTM layers was activated in order for each layer to return the complete output sequence for each sequence entry instead than only the last output. In other words, each LSTM layer would return as output a tri-dimensional sequence of the shape (batch size, time steps, units) instead of just a bi-dimensional layer of the form (batch size, units). This decision is made to capture the complex temporal dependencies that could exists in the complete signals.
- **Flattening and Dense layers:** After the LSTM layers, the output sequence is flattened to transform it in a one dimensional vector which is necessary for the next Dense layers. The first Dense layer has 128 neurons interconnected, the second has 64 neurons and the third has 32 neurons. In each Dense layer a 20% Dropout rate was applied.
- **Output layer:** The network ends with a Dense layer with just one neuron and a sigmoid activation function ideal for binary classification as it produces an output in the range [0,1], which is interpreted as a probability to belong to the positive layer.

On the other side, the **hybrid architecture of the CNN-LSTM model** has the following important elements:

- **Convolutional layers:** The convolutional part is composed of two Conv1D blocks. The first block is composed of 256 filters, while the second one has 128 filters. In both cases a kernel size = 3 and a Leaky ReLU activation function were used. These layers look for the extraction of local features from the input signal. In both blocks a MaxPooling1D was used with a pooling size = 2. This

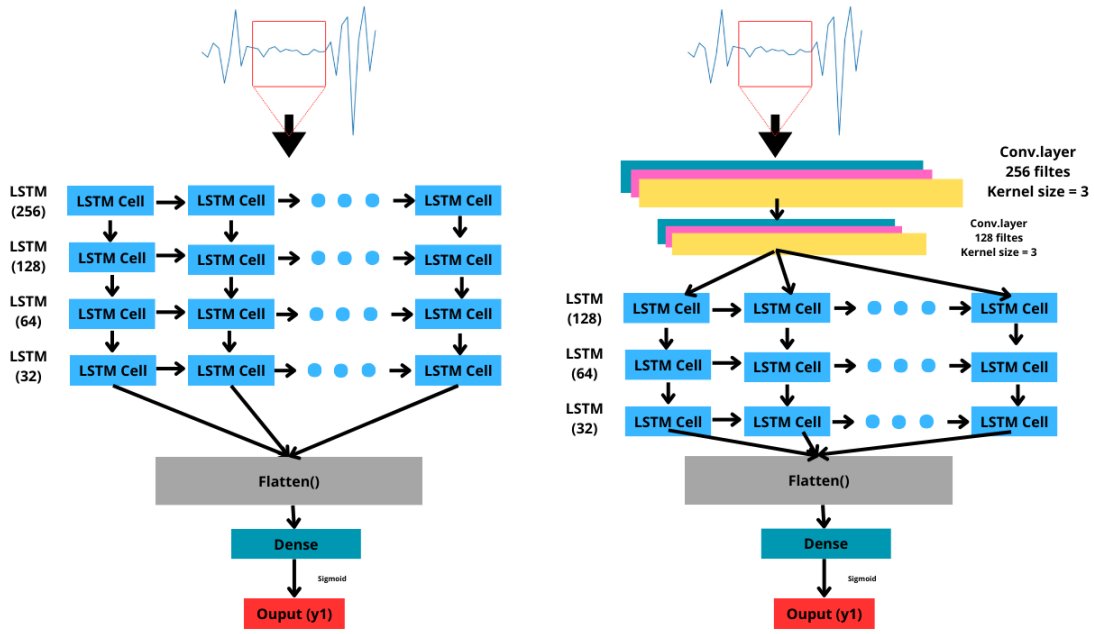

Figure 4.7: LSTM (left) and CNN-LSTM(right) architecture model blocks representation. The multiple Dense layers where omitted to only one for reasons of simplicity in the visualization.

helps in reducing the dimensionality of the features extracted, diminishing the computational complexity and preventing the overfitting. Moreover a Batch-Normalization and a Dropout layer with 50% rate were used to prevent the overfitting by turning off random cells.

- **LSTM layers:** As in the previous LSTM model. The LSTM layers are aimed to capture the temporal dependencies between the data. In these case, as the features are obtained from temporal data they are expected to have some kind of temporal relationship that can help in the proper alternan detection. The first LSTM layer was composed of 128 units, including the sequences return to the next LSTM layer and a 20% Dropout. The second layer has the same characteristics but only including 64 units. The third layer was composed of 32 units. In every case, a ReLU activation function was used.

- **Flatten and Dense layers:** After these CNN and LSTM layers, the output is flattened to transform in a one dimensional vector. After that two 64 and 32 Dense layers were used, both with the ReLU activation function.

- **Output layer:** The final layer was a Dense unit with a sigmoid activation function.

Related to the training of both networks, the **Adam optimizer** was used with a learning rate of 1e-3 to avoid the excessive overfitting. The **binary cross-entropy loss function** is used as it is recommended for binary classification tasks.

The whole training with the LSTM network was elapsed for **50 epochs** with a **batch size = 128**. On the other side, the CNN-LSTM network was trained for **150 epochs** with the same batch size The input data corresponds to the training set together with the validation set used as control metric of the performance.

The training of both networks was assessed in a virtual environment facilitated by the public ML platform Kaggle [88]. The use of this platform attends to the need of a powerful tool to accelerate the process of the network's training and to have the possibility to perform trials in the network's structures with certain speed. Therefore, the **GPU P100** accelerator was used for this entire part.

In order to achieve an increased performance in the results obtained by the networks, an optimization of the network hyperparameters was developed. As it is expected, explore the whole possible hyperparemeter space of a network of these dimensions constitutes an impossible challenge as the combinations increase exponentially when adding multiple layers. To face this challenge, the tool keras.hyperparameter was used, especially the RandomSearch tool which allows for an efficient exploration of the hyperparameter space.

In order to make sure the conservation of the best possible model during the training, the keras function *"ModelCheckpoint"* which stores the best model based on the validation set, monitoring the validation accuracy metric during the training was employed.

Chapter 5

Results and Discussion

5.1 Machine Learning results

As explained in the experimental section a Five-fold CV algorithm was used to define the best possible hyperparameters for each of the different algorithms. The hyperparameters resulted from this procedure for each of the ML algorithms can be visualized in table 7.1 for the random TWA amplitude dataset, which at the end are the same than for the 30 μV dataset. For each of the following algorithms, these hyperparameters were used to increase the models performances.

Once the hyperparameters were already defined, the models were trained and tested using the disjoint training and test sets. For each of the models the following performance metrics have been used in order to check the capabilities of the models in different aspects: **Accuracy, specificity, sensitivity, f1 score, PPV and AUC**. The performance metrics for each of the models and for both experiments can be visualized in table 5.1. As a matter of congruence for fair comparison between algorithms the same training and test set were used for every model.

Since in this study, an experiment using alternating signals with amplitudes of 30 μV, as well as randomly selected alternating signals within the range of 30 to 70 μV were conducted, one of the main objective was to assess the model's ability to detect low-amplitude alternans ($30\mu V$) as well as alternans amplitude variations which are more similar to real clinical conditions.

As it can be observed in table 5.1, the results obtained with the $30\mu V$ alternation dataset were less satisfactory, likely due to the low amplitude of the signals. However, in the experiment with random alternations, we found that errors associated with low-amplitude alternations were offset by successes in alternations with larger

amplitudes, leading to overall more promising results.

Based on these findings, we will focus future discussions solely on the results obtained in the variable amplitude experiment. This is because the results from the $30\mu V$ signal experiment are showing the same shape behaviour but with less performance in all the related metrics. This analysis has sense as $30\mu V$ is a very low amplitude to be detected so it was expected to obtain these results.

The first algorithm tried is the **Logistic Regression**. The sklearn function *LogisticRegression* was used. The confusion matrix from the test set predictions in figure 5.1. This algorithm stands out for having the best accuracy, 90.08%, over the four algorithms tried in this framework, showing a good trade off between specificity 89.07% and sensitivity 91.22%. In this algorithm, the hyperparemter *penalty* was analysed using the previously mentioned procedure.

Figure 5.1: Confusion matrix on test set obtained with the Logistic Regression model. Random TWA amplitude (left) and $30\mu V$ TWA amplitude (right).

Following, a **Decision Tree** algorithm was tried. In these model, the following hyperparameters were analysed: *min samples leaf* and *criterion*. This algorithm showed the results in figure 5.2. As it can be seen this model shows a **great sensitivity metric result,** 96.40%. However, this high performance on sensitivity is compensated with the lowest specificity over the models studied with 78.41%. The election of this algorithm would depend, therefore, on the goals pursued, as this model stands out in the detection of TWA containing signals with only 609 cases considered as non-TWA containing signals from a complete set of 35899 signals.

The next algorithm tested in this work was the so-called **Random Forest** algorithm. In this case, the *min samples leaf* and *criterion* hyperparameters were analysed. This algorithm did not stand out in any of the related metrics. However, it can be appreciated that the decision made by a bunch of trees improve the speci-

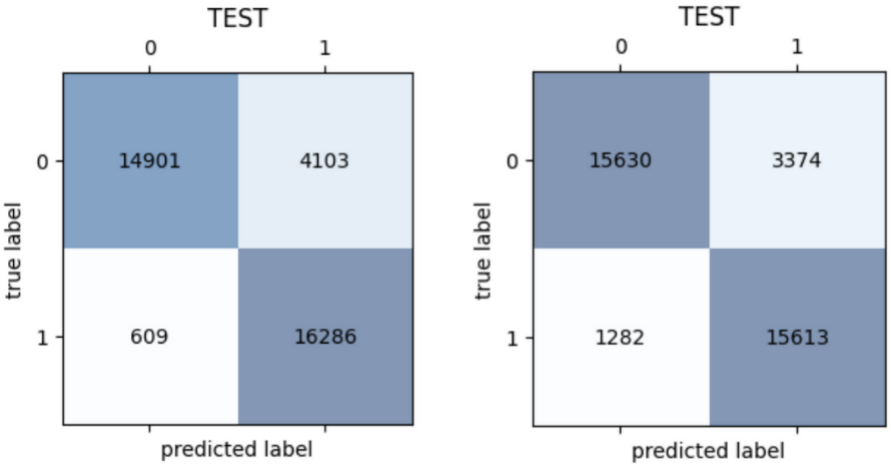

Figure 5.2: Confusion matrix on test set obtained with the Decision Tree model. Random TWA amplitude (left) and $30\mu V$ TWA amplitude (right).

ficity than just one single tree offering a more balanced model than the DT in terms of specificity-sensitivity trade off.

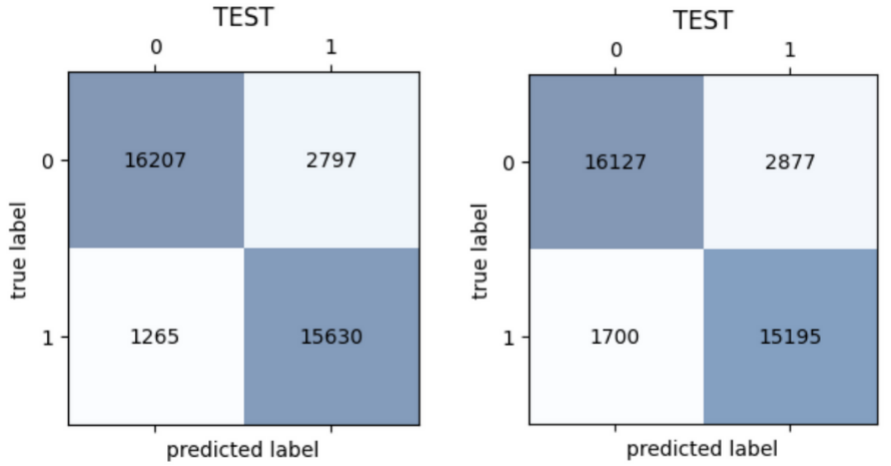

Figure 5.3: Confusion matrix on test set obtained with the Random Forest model. Random TWA amplitude (left) and $30\mu V$ TWA amplitude (right).

Finally, a **Support Vector Machine** algorithm was analysed. The following hyperparameters were studied to get the best performance of it: *Kernel* and *gamma*. In figure 5.4, the confusion matrix results can be visualized. The SVM model show a great general performance with an 87% accuracy. It specially stands out for having a great sensitivity of 95% (second among ML algorithms), showing a great capacity to detect TWA signals. However, as with the DT, there is a lack of reliable specificity with an 83%.

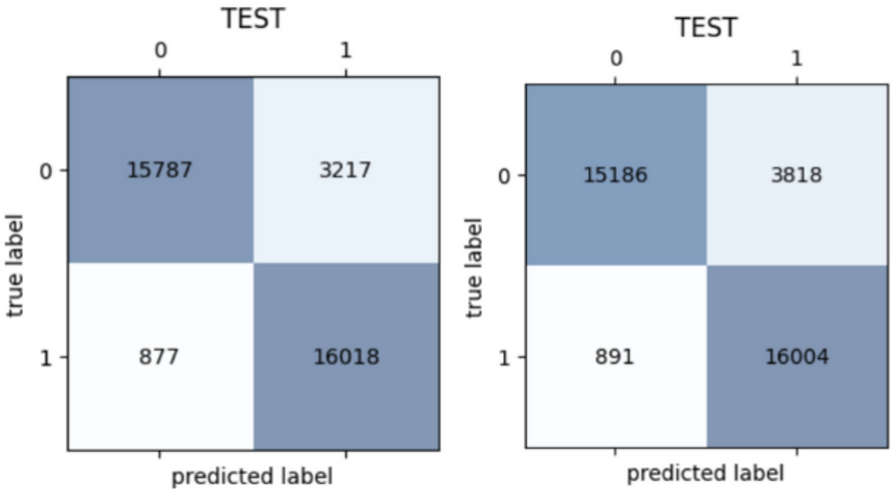

Figure 5.4: Confusion matrix on test set obtained with the SVM model. Random TWA amplitude (left) and $30\mu V$ TWA amplitude (right).

5.2 Deep Learning results

This section will cover the results obtained thanks to the training of the LSTM and CNN-LSTM networks seen in figure 4.7. As said, the networks parameters were finne-tunned thanks to the use of the keras hyperparameter tuner. The parameters used for the LSTM and the CNN-LSTM networks can be seen in tables 7.2 and 7.3, respectively. Furthermore, as it was seen in the previous section, the results on the $30\mu V$ amplitude experiment and the random amplitude experiment show a similar behaviour. Thus, for reasons of simplicity and with the goal of being coherent with clinical cases where the amplitudes of the TWA may be different, the networks where trained with random amplitude TWA signals.

In the case of the LSTM network the total training time for 50 epochs using a batch size = 128 and with the use of the GPU P1000 was of **12.5 minutes**, which shows a great capability of this model to quickly train even though the big amount of data. This great velocity of training derived also in a great predicting speed; just **8 seconds for the prediction of 35899 signals**, which supposes a great advantage in a real clinical scenario providing versatility to the model.

The model's loss and model's accuracy for both the training set and the validation set can be seen in figure 5.5. These figures show the great capability of the model to rapidly get enough information to make predictions on the validation test with almost a 92% accuracy in a very low number of epochs. However, it can be seen that throughout the training there are some falls in the progress attending to possible vanishing gradient problems. However, thanks to the use of the LSTM cells there was a quick recovery after these falls which turn on in a continuous process of learning throughout the training.

	LR	**DT**	**RF**	**SVM**
Random TWA amplitude experiment				
Accuracy	**0.908**	0.868	0.886	0.886
Sensitivity	0.912	**0.964**	0.925	0.948
Specificity	**0.89**	0.784	0.852	0.830
PPV	**0.881**	0.799	0.848	0.832
f1 score	**0.896**	0.873	0.825	0.886
AUC	**0.97**	0.95	0.96	0.96
30 μV experiment				
Accuracy	**0.875**	0.87	0.872	0.868
Sensitivity	0.877	0.924	0.90	**0.947**
Specificity	**0.873**	0.822	0.848	0.799
PPV	**0.861**	0.822	0.84	0.807
f1 score	**0.869**	0.87	0.869	0.817
AUC	0.95	0.95	0.95	0.95

Table 5.1: Table comparing the performance of Logistic Regression (LR), Decision Tree (DT), Random Forest (RF) and Support Vector Machine (SVM) for the metrics of accuracy, sensitivity, specificity, PPV, f1 score and AUC for both experiments.

Once the training was completed, the predictions on the test set resulted in the confusion matrix of figure 5.6.

To maximize the trade-off between specificity and sensitivity, the **Youden index** was used to select the optimal threshold to decide from which probability a prediction should be classified as positive. The Youden index, J, is defined as:

$$J = \text{Sensitivity} + \text{Specificity} - 1 \tag{5.1}$$

By calculating the Youden index for each possible threshold, we can identify the threshold that maximizes J, ensuring the best balance between Sensitivity and Specificity. This optimal threshold was then used to make the classification decision, aiming to improve the overall performance of this diagnostic test.

Continuing with the CNN-LSTM network, the same procedure of training was developed, however, in this case, since obtaining features diminishes the rate of learning, a total of 150 epochs were set as training time to guarantee a complete network training. The whole procedure elapsed for a total time of **17.5 minutes**, which is even a faster than the one in the LSTM network. As expected, this faster training time was reflected also in the predictions time with just 4 seconds to make the whole bunch of signals analysis. Again, the models training curves can be seen in figure 5.7:

In this case, in contrast to the previous network, there are not important falls in the development of the training since the features selected by the CNN guarantees that the LSTM networks are always receiving information and dismissing, therefore,

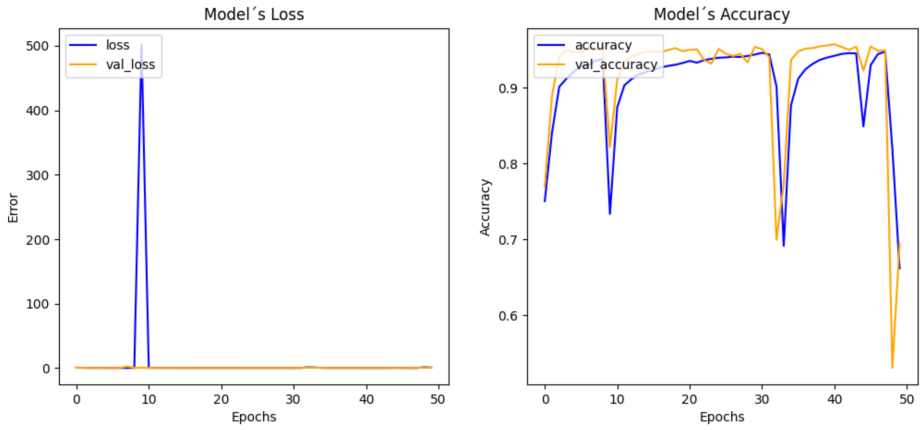

Figure 5.5: Model's loss (left) and Model's accuracy (right) of the LSTM network training process for both the training and the validation set.

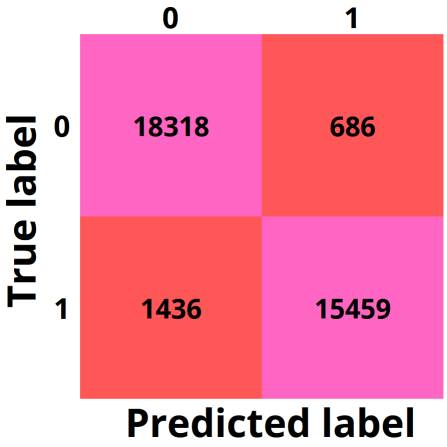

Figure 5.6: Confusion matrix on the test set predicted by the LSTM network.

the probabilities of a big gradient vanishing. The results obtained in the predictions are available in the confusion matrix of figure 5.8:

In order to have a good comparison between the models, the table 5.2 of metrics can be consulted.

	Acc	**Sens**	**Spec**	**f1**	**PPV**	**AUC**
LSTM	**0.9408**	0.9152	0.9639	0.935	0.957	0.98
CNN-LSTM	0.9257	0.8971	0.9511	0.917	0.941	0.98

Table 5.2: Table of results for the LSTM and CNN-LSTM networks where acc, sens and spec describes accuracy, sensitivity and specificity respectively.

As it can be seen, the LSTM networks surpasses the CNN-LSTM architecture in every studied metric with an outstanding **94.08% accuracy**. Moreover, in both cases the specificity has a superior value compared to the sensitivity, in other words, both DL networks (in contrast with what happened in the ML algorithms), show

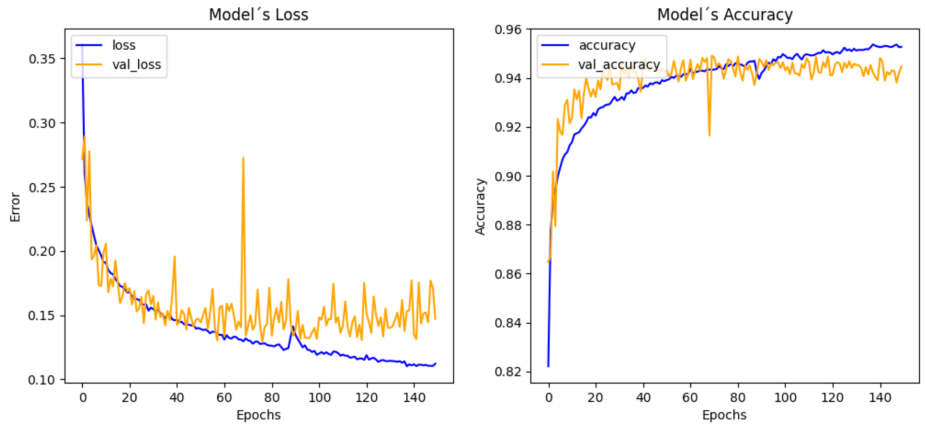

Figure 5.7: Model's loss (left) and Model's accuracy (right) of the CNN-LSTM network training process for both the training and the validation set.

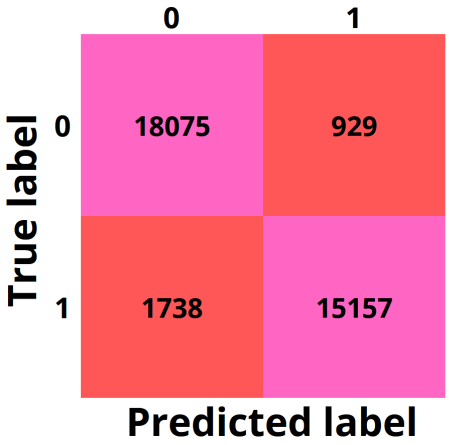

Figure 5.8: Confusion matrix on the test set predicted by the CNN-LSTM network.

a great capacity (**96.39% and 95.11%**) in identifying the patients that are not suffering from the alterning phenomena.

5.3 Discussion

The analysis of the different ML algorithms shows significant variations on the performance metrics, which are essential to determine the applicability of each model in TWA in ECG signals detection tasks. In this sense, the logistic regression stood out for having the best balance over the models (91.22% sensibility and 89.07% specificity), being efficient both in the TP and FN detection. In contrast, the **DT showed the best sensibility** (96.40%) over all the models (including DL), which indicates an amazing capability in the detection of TWA signals. However, its specificity was the lowest among all the models (78.41%). This model would be ideal in cases where it is crucial to minimize the FN, although there would be an

increase in the FP. Finally, RF and the SVM did not stand out in any related metric compared to the last two models.

Continuing now with the DL models, they have shown an increased performance compared to the ML algorithms in the TWA detection task. The LSTM networks obtained **an outstanding accuracy of 94.08%** and improved the performance of the CNN-LSTM in every of the studied metrics. This indicates that the LSTM showed better capability to manage temporal dependencies with the entire signals as inputs than with the CNN extracted features as input. In both networks, the training and the prediction times where sufficiently low to allow a good reproducibility of the experiments.

As a final remark, it is important to compare the work done with previous works in the field. In section 2.6, it was seen that some works on the area of ML applied to the TWA signals were done in the past years, reporting an 88% accuracy with the DT model [4], which surpasses the accuracy of 79% obtained with the SM. With this work, we have not only surpassed the metrics of the SM but also improved upon the results obtained in recent literature.

This work goes beyond this by incorporating and summarizing not only ML technique but also DL methodologies that have shown a superior performance in the cardiac signal analysis. The results obtained with DL models, especially with the LSTM network prove a considerable improvement in the TWA detection compared to previous works which states a new standard in this field of study.

Chapter 6

Conclusions, future work and competencies acquired

In this work, the use of ML and DL techniques for the automatic detection of TWA in ECG signals has been explored. The results obtained have shown that LSTM networks present a significant superior performance compared with the traditional ML models. Thanks to this study, four main conclusions can be obtained:

1. **Model's efficacy**: The LSTM networks reached an accuracy of **94.08%**, surpassing the combined CNN-LSTM networks in all the studied metrics. This highlighted the capacity of LSTM networks to manage temporal dependencies in ECG signals, capturing better the TWA than traditional ML algorithms.

2. **Comparison with previous works**: When comparing this work with previous studies, an improvement in the TWA detection was observed. While previous investigations report an accuracy of 88%, this methodology achieves a **new standard in the TWA detection field**.

3. **Capacity of integrating this model in a real-time clinical scenario**: Thanks to the low predictions times of this LSTM model (8 seconds for the prediction of 35899 signals), the application in clinical settings where the velocity is crucial to apply correct preventive techniques is possible.

4. **SCD prevention**: As stated, SCD is highly correlated with the alternans phenomena. SCD constitutes one the leading cause of mortality worldwide. Thanks to this study, a new reliable way of preventing this pathology arises.

Despite from the advances developed in the field, there are some areas of improvement and expansion.

1. **Databases increase**: During the work, the lack of reliable databases has been one of the critical points in this study. An increase in these types of databases with real TWA signals is necessary to increase the generalization and robustness of these types of models.

2. **Model optimization**: To explore and to optimize other DL architectures may lead to improvements in the related metrics. The use of transfer learning techniques and the increase in computational resources may lead to this task.

3. **Other types of alternans analysis**: In this work, only sustained alternans were added to the ECG signals. This, may lead to a lack of generalization of this work in clinical scenarios.

4. **Distinction between discordant and concordant alternans:** As said, the risk of developing SCD, VT or VF increase when there is a transition from concordant to discordant alternates. Further works on distinguishing between these two alternans shapes may lead to a more complete understanding of the phenomena leading to a prevention of these diseases.

These limitations suggest new lines of work that may be investigated in future studies. By the time, this works has tried to give a new step towards the prevention of cardiovascular diseases through TWA analysis.

Regarding the competences acquired, thanks to the development of this final degree project, I have been able to apply many of the skills and competencies acquired during my degree in Biomedical Engineering. Courses such as Physiological Signal Processing, Linear and Discrete Systems, Biological Systems Analysis, and Medical Pathology have allowed me to understand and apply concepts related to alternating waves, ECG analysis, and even the application of complex operations on real time signals. Furthermore, thanks to a strong background in mathematics, programming, physics, and optimization, combined with specific skill acquired in courses such as biomedical equipment, hospital engineering, artificial intelligence, and medical image analysis, I have been able to complement this work and take it to a higher level. Undoubtedly, this project has been completed thanks to significant effort and good content planning throughout my four years of studying Biomedical Engineering.

Bibliography

[1] Lüscher, T. F. (2016). Prevention: some important steps forward, but many unmet needs in a world with cardiovascular disease as the leading cause of death. European Heart Journal, 37(42), 3179–3181. https://doi.org/10.1093/eurheartj/ehw566

[2] Kumar A, Avishay DM, Jones CR, Shaikh JD, Kaur R, Aljadah M, Kichloo A, Shiwalkar N, Keshavamurthy S. Sudden cardiac death: epidemiology, pathogenesis and management. Rev Cardiovasc Med. 2021 Mar 30;22(1):147-158. doi: 10.31083/j.rcm.2021.01.207. PMID: 33792256.

[3] Kochi AN, Vettor G, Dessanai MA, Pizzamiglio F, Tondo C. Sudden Cardiac Death in Athletes: From the Basics to the Practical Work-Up. Medicina (Kaunas). 2021 Feb 14;57(2):168. doi: 10.3390/medicina57020168. PMID: 33673000; PMCID: PMC7918885.

[4] Fernández-Calvillo MG, Goya-Esteban R, Cruz-Roldán F, Hernández-Madrid A, Blanco-Velasco M. Machine Learning approach for TWA detection relying on ensemble data design. Heliyon. 2023 Jan 16;9(1):e12947. doi: 10.1016/j.heliyon.2023.e12947. PMID: 36699267; PMCID: PMC9868537.

[5] Zipes DP, Wellens HJ. Sudden cardiac death. Circulation. 1998 Nov 24;98(21):2334-51. doi: 10.1161/01.cir.98.21.2334. PMID: 9826323.

[6] Wong CX, Brown A, Lau DH, Chugh SS, Albert CM, Kalman JM, Sanders P. Epidemiology of Sudden Cardiac Death: Global and Regional Perspectives. Heart Lung Circ. 2019 Jan;28(1):6-14. doi: 10.1016/j.hlc.2018.08.026. Epub 2018 Sep 24. PMID: 30482683.

[7] Kumar A, Avishay DM, Jones CR, Shaikh JD, Kaur R, Aljadah M, Kichloo A, Shiwalkar N, Keshavamurthy S. Sudden cardiac death: epidemiology, pathogenesis and management. Rev Cardiovasc Med. 2021 Mar 30;22(1):147-158. doi: 10.31083/j.rcm.2021.01.207. PMID: 33792256.

[8] de Vreede Swagemakers JJM, Gorgels APM, Dubois-Arbouw WI, van Ree JW, Daemen MJAP, Houben LGE, Wellens HJJ. Out-of-hospital cardiac arrest in the 1990's: a population-based study in the Maastricht area on incidence, characteristics and survival. J Am Coll Cardiol.1997; 30:1500–1505.

[9] Gimeno-Blanes FJ, Blanco-Velasco M, Barquero-Pérez Ó, García-Alberola A, Rojo-Álvarez JL. Sudden Cardiac Risk Stratification with Electrocardiographic Indices - A Review on Computational Processing, Technology Transfer, and Scientific Evidence. Front Physiol. 2016 Mar 7;7:82. doi: 10.3389/fphys.2016.00082. PMID: 27014083; PMCID: PMC4780431.

[10] Goldberger, J. J., Cain, M. E., Hohnloser, S. H., Kadish, A. H., Knight, B. P., Lauer, M. S., et al. (2008). American heart association/american college of cardiology foundation/heart rhythm society scientific statement on noninvasive risk stratification techniques for identifying patients at risk for sudden cardiac death: a scientific statement from the american heart association council on clinical cardiology committee on electrocardiography and arrhythmias and council on epidemiology and prevention. Circulation 118, 1497–1518. doi: 10.1161/CIRCULATIONAHA 107.189375

[11] Nerbonne JM, Kass RS. Molecular physiology of cardiac repolarization. Physiol Rev. 2005 Oct;85(4):1205-53. doi: 10.1152/physrev.00002.2005. PMID: 16183911.

[12] Petmezas G, Stefanopoulos L, Kilintzis V, Tzavelis A, Rogers JA, Katsaggelos AK, Maglaveras N. State-of-the-Art Deep Learning Methods on Electrocardiogram Data: Systematic Review. JMIR Med Inform. 2022 Aug 15;10(8):e38454. doi: 10.2196/38454. PMID: 35969441; PMCID: PMC9425174.

[13] Fu DG. Cardiac Arrhythmias: Diagnosis, Symptoms, and Treatments. Cell Biochem Biophys. 2015 Nov;73(2):291-296. doi: 10.1007/s12013-015-0626-4. PMID: 25737133.

[14] Somani S, Russak AJ, Richter F, Zhao S, Vaid A, Chaudhry F, De Freitas JK, Naik N, Miotto R, Nadkarni GN, Narula J, Argulian E, Glicksberg BS. Deep learning and the electrocardiogram: review of the current state-of-the-art. Europace. 2021 Aug 6;23(8):1179-1191. doi: 10.1093/europace/euaa377. PMID: 33564873; PMCID: PMC8350862.

[15] Sajeev JK, Koshy AN, Teh AW. Wearable devices for cardiac arrhythmia detection: a new contender? Intern Med J. 2019 May;49(5):570-573. doi: 10.1111/imj.14274. PMID: 31083804.

[16] Anas, Emran Lee, Soo Hasan, Md. (2010). Sequential algorithm for life threatening cardiac pathologies detection based on mean signal strength and EMD functions. Biomedical engineering online. 9. 43. 10.1186/1475-925X-9-43.

[17] Edwards JN, Blatter LA. Cardiac alternans and intracellular calcium cycling. Clin Exp Pharmacol Physiol. 2014 Jul;41(7):524-32. doi: 10.1111/1440-1681.12231. PMID: 25040398; PMCID: PMC4122248.

[18] Traube L. Ein Fall von Pulsus Bigeminus nebst Bemerkungen uber die Leberschwellungen bei Klappenfehlern and uber acute Leberatrophie. Berlin Klin Wochenschr. 1872;9:185–8

[19] Hering HE. Das Wesen des Herzalternans. Munchen Med Wochenshr 1908;4:1417–21.

[20] Lewis T. Notes upon alternation of the heart. Q J Med 1910;4: 141–4

[21] Kalter HH, Schwartz ML. Electrical alternans. N Y State J Med 1948;1:1164–6.

[22] Goya-Esteban R, Barquero-Pérez O, Blanco-Velasco M, Caamaño-Fernández AJ, García-Alberola A, Rojo-Álvarez JL. Nonparametric signal processing validation in T-wave alternans detection and estimation. IEEE Trans Biomed Eng. 2014 Apr;61(4):1328-38. doi: 10.1109/TBME.2014.2304565. PMID: 24658256.

[23] Cutler MJ, Rosenbaum DS. Explaining the clinical manifestations of T wave alternans in patients at risk for sudden cardiac death. Heart Rhythm. 2009 Mar;6(3 Suppl):S22-8. doi: 10.1016/j.hrthm.2008.10.007. Epub 2008 Oct 10. PMID: 19168395; PMCID: PMC2680220.

[24] Kaufman ES, Mackall JA, Julka B, et al. Influence of heart rate and sympathetic stimulation on arrhythmogenic T wave alternans. Am J Physiol Heart Circ Physiol. 2000;279:H1248–H1255. [PubMed] [Google Scholar]

[25] Qu Z, Garfinkel A, Chen P, et al. Mechanisms of discordant alternans and induction of reentry in simulated cardiac tissue. Circulation. 2000;102:1664–1670. [PubMed] [Google Scholar] [Ref list]

[26] Watanabe MA, Fenton FH, Evans SJ, et al. Mechanisms for discordant alternans. J Cardiovasc Electrophysiol. 2001;12:196–206. [PubMed] [Google Scholar] [Ref list]

[27] Fox JJ, McHarg JL, Gilmour RF Jr. Ionic mechanism of electrical alternans. Am J Physiol Heart Circ Physiol. 2002 Feb;282(2):H516-30. doi: 10.1152/ajpheart.00612.2001. PMID: 11788399.

[28] Schwartz PJ, Malliani A. Electrical alternation of the T-wave: clinical and experimental evidence of its relationship with the sympathetic nervous system and with the long Q-T syndrome. Am Heart J. 1975;89:45–50. [PubMed] [Google Scholar] [Ref list]

[29] Miyoshi S, Miyazaki T, Moritani K, Ogawa S. Different responses of epicardium and endocardium to KATP channel modulators during regional ischemia. Am J Physiol. 1996 Jul;271(1 Pt 2):H140-7. doi: 10.1152/ajpheart.1996.271.1.H140. PMID: 8760169.

[30] Steenbergen C, Murphy E, Watts JA, London RE. Correlation between cytosolic-free calcium, contracture, ATP, and irreversible ischemic injury in perfused rat heart. Circ Res 1990;66:135–46

[31] TC, Angelakos ET, Schaffer SW. Relationship between adenine nucleotide metabolism and irreversible ischemic tissue damage in isolated perfused rat heart. Circ Res 1979;45:218–25

[32] Marba´n E, Kitakaze M, Koretsune Y, Yue DT, Chacko VP, Pike MM. Quantification of [Ca2]i in perfused hearts. Critical evaluation of the 5F-BAPTA and nuclear magnetic resonance method as applied to the study of ischemia and reperfusion. Circ Res 1990;66: 1255–67.

[33] Armoundas AA, Tomaselli GF, Esperer HD. Pathophysiological basis and clinical application of T-wave alternans. J Am Coll Cardiol. 2002 Jul 17;40(2):207-17. doi: 10.1016/s0735-1097(02)01960-5. PMID: 12106921.

[34] QuZ, GarfinkelA, ChenP, WeissJ. Mechanisms of discordant alternans and induction of reentry in simulated cardiac tissue, Circulation, 2000, vol. 102(pg. 1664-70)

[35] Pastore JM, Girouard SD, Laurita KR, et al. Mechanism linking T-wave alternans to the genesis of cardiac fibrillation. Circulation. 1999;99:1385–1394.

[36] Lance D. Wilson, David S. Rosenbaum, Mechanisms of arrythmogenic cardiac alternans, EP Europace, Volume 9, Issue suppl, November 2007, Pages vi77–vi82, https://doi.org/10.1093/europace/eum210

[37] Suzuki K, Murtuza B, Smolenski RT, Sammut IA , Suzuki N, Kaneda Y, et al. Cell transplantation for the treatment of acute myocardial infarction using vascular endothelial growth factor-expressing skeletal myoblasts, Circulation, 2001, vol. 104(pg. I207-I1212)

[38] Pastore JM, Rosenbaum DS. Role of structural barriers in the mechanism of alternans-induced reentry, Circ Res, 2000, vol. 87 (pg. 1157-63)

[39] Tanno, K., Kobayashi, Y., Adachi, T., Ryu, S., Asano, T., Obara, C., et al. (2000).Onset heart rate and microvolt T–wave alternans during atrial pacing. Am. J.Cardiol. 86, 877–880. doi: 10.1016/S0002-9149(00)01111-5

[40] Verrier, R. L., Klingenheben, T., Malik, M., El-Sherif, N., Exner, D. V., Hohnloser,S. H., et al. (2011). Microvolt T–wave alternans: physiological basis, methods of measurement, and clinical utility—consensus guideline by international society for holter and noninvasive electrocardiology. J. Am. Coll. Cardiol. 58, 1309–1324. doi: 10.1016 j.jacc.2011.06.029

[41] Rosenbaum, D. S., Albrecht, P., and Cohen, R. J. (1996). Predicting sudden cardiac death from T wave alternans of the surface electrocardiogram: promise and pitfalls. J. Cardiovasc. Electrophysiol. 7, 1095–1111. doi: 10.1111/j.1540-8167.1996.tb00487.x

[42] Nearing, B. D., and Verrier, R. L. (2002). Modified moving average analysis of T–wave alternans to predict ventricular fibrillation with high accuracy. J. Appl.Physiol. 92, 541–549. doi: 10.1152/japplphysiol.00592.2001

[43] L. Burattini, S. Bini, R. Burattini, Comparative analysis of methods for automatic detection and quantification of microvolt T-wave alternans, Med. Eng. Phys. 31 (10) (2009) 1290–1298.

[44] L. Burattini, S. Bini, R. Burattini, Correlation method versus enhanced modified moving average method for automatic detection of T–wave alternans, Comput.Methods Programs Biomed. 98 (1) (2010) 94–102.

[45] Verrier, R. L., Klingenheben, T., Malik, M., El-Sherif, N., Exner, D. V., Hohnloser, S. H., et al. (2011). Microvolt T–wave alternans: physiological basis, methods of measurement, and clinical utility—consensus guideline by international society for holter and noninvasive electrocardiology. J. Am. Coll. Cardiol. 58, 1309–1324. doi: 10.1016/j.jacc.2011.06.029

[46] Reddy, Y. C. A. P., Viswanath, P., Reddy, B. E. (2018). Semi-supervised learning: A brief review. Int. J. Eng. Technol, 7(1.8), 81

[47] Anavi Y, Kogan I, Gelbart E, Geva O, Greenspan H (2015) A comparative study for chest radiograph image retrieval using binary texture and deep learning classification. In: Proceedings of the IEEE engineering in Medicine and Biology Society, pp 2940–2943. https://doi.org/10.1109/EMBC.2015.7319008

[48] Paz, Hellen Maia, Mateus Moraes, Fernando Lustosa, Ricardo Costa, Lilia Macêdo, Samuel Barreto, Marcos Ara, Anderson. (2020). Local Processing of Massive Databases with R: A National Analysis of a Brazilian Social Programme. Stats. 3. 10.3390/stats3040028.

[49] Huang S, Cai N, Pacheco PP, Narrandes S, Wang Y, Xu W. Applications of Support Vector Machine (SVM) Learning in Cancer Genomics. Cancer Genomics Proteomics. 2018 Jan-Feb;15(1):41-51. doi: 10.21873/cgp.20063. PMID: 29275361; PMCID: PMC5822181.

[50] Aizerman MA, Braverman EM, Rozoner LI. Theoretical foundations of the potential function method in pattern recognition learning. Autom Remote Control. 1964;25:821–837. [Google Scholar]

[51] ROBERT HECHT-NIELSEN,III.3 - Theory of the Backpropagation Neural Network**Based on "nonindent" by Robert Hecht-Nielsen, which appeared in Proceedings of the International Joint Conference on Neural Networks 1, 593–611, June 1989. © 1989 IEEE.,Editor(s): Harry Wechsler,Neural Networks for Perception,Academic Press,1992,Pages 65-93,ISBN 9780127412528,https://doi.org/10.1016/B978-0-12-741252-8.50010-8.

[52] P. P. Shinde and S. Shah, "A Review of Machine Learning and Deep Learning Applications," 2018 Fourth International Conference on Computing Communication Control and Automation (ICCUBEA), Pune, India, 2018, pp. 1-6, doi: 10.1109/ICCUBEA.2018.8697857.

[53] T. Lindeberg, "Scale invariant feature transform," Scholarpedia, vol. 7, no. 5, p. 10491, May 2012.

[54] Z. Li, F. Liu, W. Yang, S. Peng and J. Zhou, "A Survey of Convolutional Neural Networks: Analysis, Applications, and Prospects," in IEEE Transactions on Neural Networks and Learning Systems, vol. 33, no. 12, pp. 6999-7019, Dec. 2022, doi: 10.1109/TNNLS.2021.3084827.

[55] Goodfellow I, Bengio Y, Courville A, Bengio Y. Deep learning, vol. 1. Cambridge: MIT press; 2016

[56] Mohammed Alsumaidaee YA, Yaw CT, Koh SP, Tiong SK, Chen CP, Yusaf T, Abdalla AN, Ali K, Raj AA. Detection of Corona Faults in Switchgear by Using 1D-CNN, LSTM, and 1D-CNN-LSTM Methods. Sensors (Basel). 2023 Mar 14;23(6):3108. doi: 10.3390/s23063108. PMID: 36991819; PMCID: PMC10059847.

[57] Das S, Tariq A, Santos T, Kantareddy SS, Banerjee I. Recurrent Neural Networks (RNNs): Architectures, Training Tricks, and Introduction to Influential Research. 2023 Jul 23. In: Colliot O, editor. Machine Learning for Brain Disorders [Internet]. New York, NY: Humana; 2023. Chapter 4. PMID: 37988518.

[58] Mu, R., Zeng, X. (2019). A review of deep learning research. KSII Transactions on Internet and Information Systems (TIIS), 13(4), 1738-1764

[59] Hochreiter S, Schmidhuber J. Long short-term memory. Neural Comput. 1997 Nov 15;9(8):1735-80. doi: 10.1162/neco.1997.9.8.1735. PMID: 9377276.

[60] Hochreiter S (1998) The vanishing gradient problem during learning recurrent neural nets and problem solutions. Int J Uncertainty Fuzziness Knowledge Based Syst 6(02):107–116.

[61] https://medium.com/@imjeremyhi/understanding-recurrent-networks-part-1-simple-rnn-lstm-cc53e7475980

[62] Yoram Reich, S.V. Barai, Evaluating machine learning models for engineering problems, Artificial Intelligence in Engineering, Volume 13, Issue 3, 1999, Pages 257-272, ISSN 0954-1810, https://doi.org/10.1016/S0954-1810(98)00021-1.

[63] Park SH, Goo JM, Jo CH. Receiver operating characteristic (ROC) curve: practical review for radiologists. Korean J Radiol. 2004 Jan-Mar;5(1):11-8. doi: 10.3348/kjr.2004.5.1.11. PMID: 15064554; PMCID: PMC2698108.

[64] Madias JE. The need for studies to evaluate the reproducibility of the T-wave alternans (TWA), and the rationale for a correction index of the TWA. Indian Pacing Electrophysiol J. 2007 Aug 1;7(3):176-83. PMID: 17684576; PMCID: PMC1939870.

[65] J. P. Martinez and S. Olmos, "A robust T wave alternans detector based on the GLRT for Laplacian noise distribution," Computers in Cardiology, Memphis, TN, USA, 2002, pp. 677-680, doi: 10.1109/CIC.2002.1166863.

[66] Verrier R.L. Klingenheben T.Malik M.El-Sherif N.Exner D.V. Hohnloser S.H.Ikeda T. Martínez J.P. Narayan S.M. Nieminen T. Rosenbaum D.S. Microvolt T–wave alternans: physiological basis, methods of measurement, and clinical utility—consensus guideline by international society for holter and noninvasive electrocardiology. J. Am. Coll. Cardiol. 2011; 58: 1309-1324

[67] Karnaukh O. Karplyuk Y. Nikitiuk N. Evaluation of machine learning techniques for ECG T–wave alternans. in: IEEE 38th International Conference on Electronics and Nanotechnology. 2018: 346-350

[68] Karnaukh O. Karplyuk Y. Application of machine learning methods for artificial ECG with T–wave alternans. in: IEEE 40th International Conference on Electronics and Nanotechnology. 2020: 613-617

[69] J.P. Martínez, S. Olmos, Methodological principles of T wave alternans analysis: a unified framework, IEEE Trans. Biomed. Eng. 52 (4) (2005) 599–613.

[70] S. Bashir, A.D. Bakhshi, M.A. Maud, A template matched-filter based scheme for detection and estimation of T-wave alternans, Biomed. Signal Process. Control 13 (2014) 247–261.

[71] B. Ghoraani, S. Krishnan, R.J. Selvaraj, V.S. Chauhan, T wave alternans evaluation using adaptive time–frequency signal analysis and nonnegative matrix factorization, Med. Eng. Phys. 33 (6) (2011) 700–711.

[72] A.L. Goldberger, L.A.N. Amaral, L. Glass, J.M. Hausdorff, P.C. Ivanov, R.G. Mark, J.E. Mietus, G.B. Moody, C.-K. Peng, H.E. Stanley, PhysioBank, PhysioToolkit, and PhysioNet: components of a new research resource for complex physiologic signals, Circulation 101 (23) (2000) 215–220.

[73] G. Moody, R. Mark, The impact of the MIT-BIH arrhythmia database, IEEE Eng. Med. Biol. Mag. 20 (3) (2001) 45–50.

[74] A. Taddei, G. Distante, M. Emdin, P. Pisani, G.B. Moody, C. Zeelenberg, C. Marchesi, The European ST-T database: standard for evaluating systems for the analysis of ST-T changes in ambulatory electrocardiography, Eur. Heart J. 13 (9) (1992) 1164–1172.

[75] Martínez JP, Olmos S, Wagner G, Laguna P. Characterization of repolarization alternans during ischemia: time-course and spatial analysis. IEEE Trans Biomed Eng. 2006 Apr;53(4):701-11. doi: 10.1109/TBME.2006.870233. PMID: 16602577.

[76] P. Laguna, R. Jané and P. Caminal, "Adaptive filtering of ECG baseline wander," 1992 14th Annual International Conference of the IEEE Engineering in Medicine and Biology Society, Paris, France, 1992, pp. 508-509, doi: 10.1109/IEMBS.1992.5761083.

[77] Maria Pilar Royo y Pablo Laguna. Cancelacion de variaciones de linea de base en el ECG: estudio comparativo de diferentes tecnicas. Libro de actas XVI Congreso Anual de la Sociedad Espanola de Ingenieria Biomedica, pp. 135-138, Valencia, Septiembre 1998.

[78] Chavan, M. S., Agarwala, R. A., Uplane, M. D. (2006, February). Use of Kaiser window for ECG processing. In Proceedings of the 5th WSEAS Int. Conf. on Signal Processing, Robotics and Automation, Madrid, Spain.

[79] Guyon, I., Elisseeff, A. (2006). An Introduction to Feature Extraction. In: Guyon, I., Nikravesh, M., Gunn, S., Zadeh, L.A. (eds) Feature Extraction. Studies in Fuzziness and Soft Computing, vol 207. Springer, Berlin, Heidelberg. https://doi.org/10.1007/978-3-540-35488-8_1

[80] C. Alippi and M. Roveri, "An adaptive CUSUM-based test for signal change detection," 2006 IEEE International Symposium on Circuits and Systems, Kos, Greece, 2006, pp. 4 pp.-, doi: 10.1109/ISCAS.2006.1693942.

[81] B.E.J Manly, and D.I. MacKenzie, "A cumulative sum type of method for environmental monitoring", Enviromnetrics, vol. 11, pp. 151-166, 2000.

[82] Scikit-learn: Machine Learning in Python, Pedregosa et al., JMLR 12, pp. 2825-2830, 2011

[83] Georgios Petmezas, Kostas Haris, Leandros Stefanopoulos, Vassilis Kilintzis, Andreas Tzavelis, John A Rogers, Aggelos K Katsaggelos, Nicos Maglaveras, Automated Atrial Fibrillation Detection using a Hybrid CNN-LSTM Network on Imbalanced ECG Datasets,Biomedical Signal Processing and Control,Volume 63, 2021,102194,ISSN 1746-8094,https://doi.org/10.1016/j.bspc.2020.102194.

[84] Rai, H.M., Chatterjee, K. Hybrid CNN-LSTM deep learning model and ensemble technique for automatic detection of myocardial infarction using big ECG data. Appl Intell 52, 5366–5384 (2022). https://doi.org/10.1007/s10489-021-02696-6

[85] B. Yuen, X. Dong and T. Lu, "Inter-Patient CNN-LSTM for QRS Complex Detection in Noisy ECG Signals," in IEEE Access, vol. 7, pp. 169359-169370, 2019, doi: 10.1109/ACCESS.2019.2955738.

[86] Chollet, F., others. (2015). Keras. GitHub. Retrieved from https://github.com/fchollet/keras

[87] Martín Abadi, Ashish Agarwal, Paul Barham, Eugene Brevdo, Zhifeng Chen, Craig Citro, Greg S. Corrado, Andy Davis, Jeffrey Dean, Matthieu Devin, Sanjay Ghemawat, Ian Goodfellow, Andrew Harp, Geoffrey Irving, Michael Isard, Rafal Jozefowicz, Yangqing Jia, Lukasz Kaiser, Manjunath Kudlur, Josh Levenberg, Dan Mané, Mike Schuster, Rajat Monga, Sherry Moore, Derek Murray, Chris Olah, Jonathon Shlens, Benoit Steiner, Ilya Sutskever, Kunal Talwar, Paul Tucker, Vincent Vanhoucke, Vijay Vasudevan, Fernanda Viégas, Oriol Vinyals, Pete Warden, Martin Wattenberg, Martin Wicke, Yuan Yu, and Xiaoqiang Zheng. TensorFlow: Large-scale machine learning on heterogeneous systems, 2015. Software available from tensorflow.org.

[88] https://www.kaggle.com

Chapter 7

Appendices

In the following sections some interesting figures and tables that support the explanations throughout the work could be seen for further understanding.

7.1 Feature selection

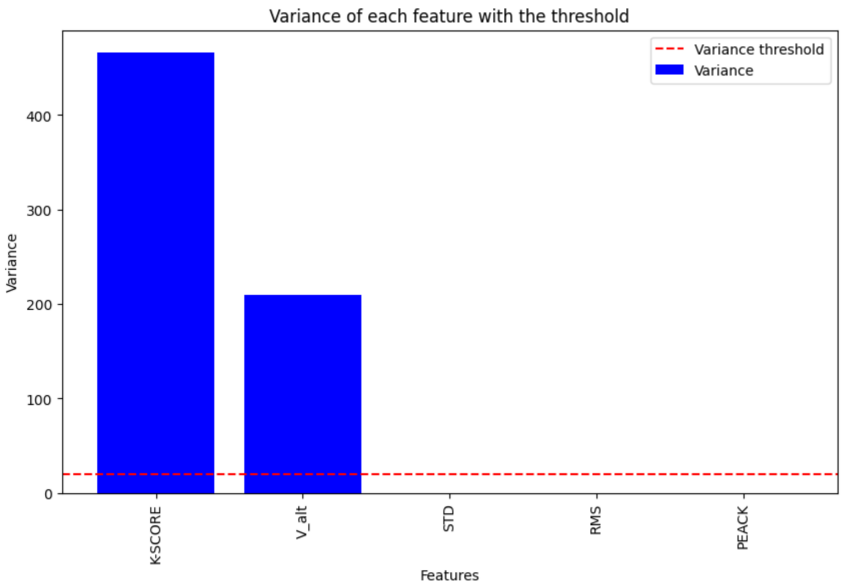

Figure 7.1: Variance thresholding selection method results applied to the continuous features.

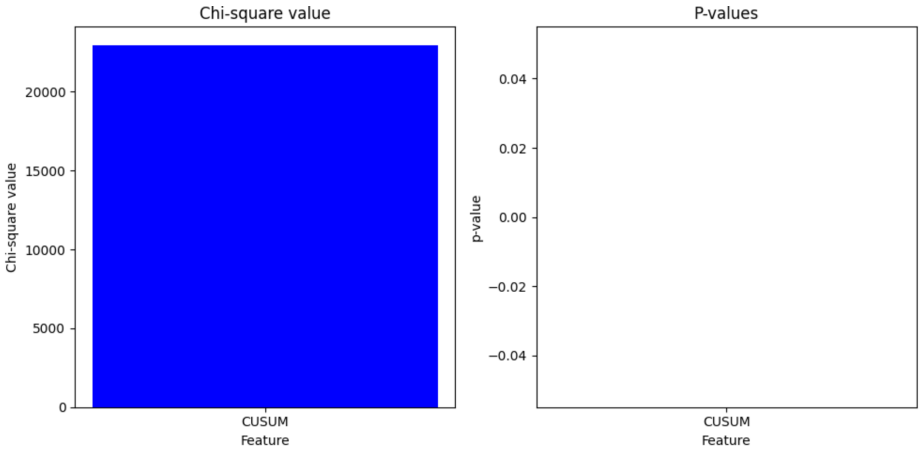

Figure 7.2: Chi-squared value (left) and p-value (right) for the CUSUM feature.

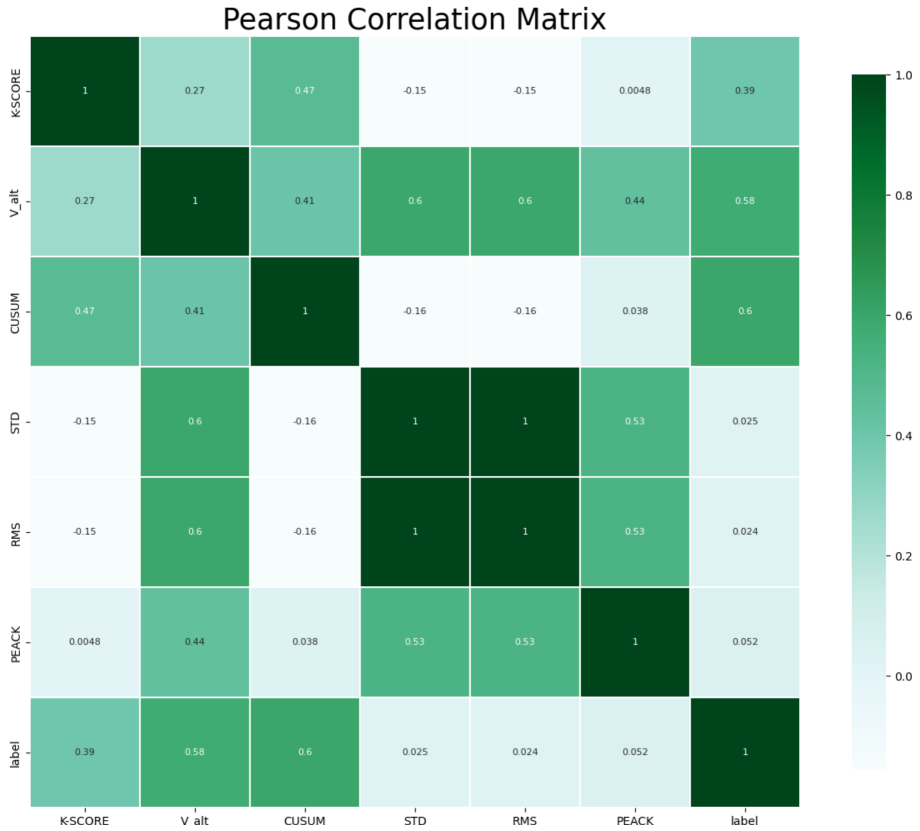

Figure 7.3: Pearson's correlation matrix on the dataset features and the label.

7.2 Machine Learning and Deep Learning results

The tables with the hyperparameters for both sections are available in this section.

	LR	**DT**	**RF**	**SVM**
Penalty	l2	-	-	-
Min Samples Leaf	-	5029	5029	-
Criterion	-	entropy	entropy	-
Kernel	-	-	-	rbf
Gamma	-	-	-	auto

Table 7.1: Table comparing hyperparameters for Logistic Regression (LR), Decision Tree (DT), Random Forest (RF), and Support Vector Machine (SVM).

Layer Type	Hyperparameters	Values
LSTM 1	Units	256
	Activation	relu
	Input Shape	(32, 39)
	Return Sequences	True
Dropout 1	Rate	0.2
LSTM 2	Units	128
	Activation	relu
	Return Sequences	True
Dropout 2	Rate	0.2
LSTM 3	Units	64
	Activation	relu
	Return Sequences	True
Dropout 3	Rate	0.2
LSTM 4	Units	32
	Activation	relu
	Return Sequences	True
Dropout 4	Rate	0.2
Flatten		
Dense 1	Units	128
Dense 2	Units	64
Dropout 5	Rate	0.2
Dense 3	Units	32
Dropout 6	Rate	0.2
Dense 7	Units	1
	Activation	sigmoid
Optimizer	Type	Adam
	Learning Rate	1e-3

Table 7.2: Hyperparameters used in the LSTM network

Layer Type	Hyperparameters	Values
Conv1D 1	Filters	256
	Kernel Size	3
	Activation	relu
	Input Shape	(32, 39)
MaxPooling1D	Pool Size	2
BatchNormalization		
LeakyReLU	Negative Slope	0.01
Dropout 1	Rate	0.5
Conv1D 2	Filters	128
	Kernel Size	3
	Activation	relu
MaxPooling1D	Pool Size	2
BatchNormalization		
LeakyReLU	Negative Slope	0.01
Dropout 2	Rate	0.5
LSTM 1	Units	128
	Activation	relu
	Return Sequences	True
Dropout 3	Rate	0.2
LSTM 2	Units	64
	Activation	relu
	Return Sequences	True
Dropout 4	Rate	0.2
LSTM 3	Units	32
	Activation	relu
	Return Sequences	True
Dropout 5	Rate	0.2
Flatten		
Dense 1	Units	64
	Activation	relu
Dense 2	Units	32
	Activation	relu
Dense 3	Units	1
	Activation	sigmoid
Optimizer	Type	Adam
	Learning Rate	1e-3

Table 7.3: Hyperparameters used in the CNN-LSTM network